Atmospheric Infrared Sounder

VALIDATION OF AIRS/AMSU/HSB CORE PRODUCTS *for* Data Release Version 4.0

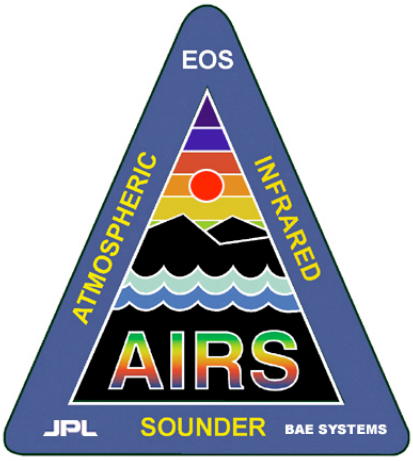

Edited by:
Eric J. Fetzer

Contributions by:

Annmarie Eldering, Evan F. Fishbein, Thomas Hearty, William F. Irion and Brian Kahn

Version 1.0

March 8, 2005
JPL D-31448

ABSTRACT

Synopsis A variety of correlative observations were compared with AIRS retrievals. Results are for latitudes in the range of 50 S to 50 N:
Cloud Cleared Radiances: Well characterized over ocean.
Surface Skin Temperature: Well characterized over ocean. Not validated over land.
Atmospheric Temperature Profiles: Well characterized over ocean, meeting 1 K per km specification. Large differences over land of ~2 K near the surface and ~1 K at altitudes of 2 km and higher.
Total Water Vapor: RMS uncertainties of oceans of ~5%. Oceanic retrievals currently flagged as highest quality include stratocumulus regions with significant moist biases. Over-land uncertainties are ~30-45%, and apparent spurious moistening in regions of high surface temperature.
Water Vapor Profiles: Meeting specification of ~15% in 2 km over oceans. Large uncertainties over land, especially in bottom 2 km of profile.
Ozone Column and Profiles: Well characterized over ocean, with agreement to a few percent. Poorer agreement over land.
Cloud Fraction and Top Pressure: Only validated over ocean. Good agreement with in situ data for low clouds.

Summary of Results This report describes validation comparisons for AIRS V4.0 retrieved data products. A detailed synopsis is given in the Executive Summary section, and individual chapters describe the analyses in detail. Comparisons are described for retrieved cloud cleared radiances, sea surface temperature (SST), temperature and humidity profiles, cloud properties and ozone.

Cloud cleared radiance are compared with clear sky radiances from ECMWF reanalyses. Channels peaking in the stratosphere and above show biases of ~0.3 K, while lower tropospheric channels have biases of ~0.4 K.

Retrieved AIRS SST are compared against ECMWF and AMSR-E, with differences of roughly -0.5 ± 0.8. The yield using Qual_Surf = 0 is low at roughly 10 percent.

Retrieved temperature profiles are compared with ECMWF and dedicated radiosondes. Root-mean-square temperature differences against ECMWF vary from about 1.3 K just above the surface to less than 1 K in the troposphere when averaged over 1 km thick layers, with biases of 0.2 K or less. Dedicated radiosondes give uncertainties of less than about 1 K in retrieved temperature in the free troposphere. Yields are height dependent, but roughly comparable to those from V3.0 in the lower troposphere. Yields are higher above, at the cost of a few tenths of a degree in performance.

Retrieved total water vapor is compared against dedicated sondes, ECMWF, and AMSR-E. The over-ocean RMS difference is 5-6% against sondes and AMSR-E. Higher RMS differences over ocean of ~12% are seen against ECMWF. Using the most stringent quality flags gives wet biases against AMSR-E in stratus regions. RMS differences in total water vapor over land vary from 31% at a single sonde site, to 43% against ECMWF.

Root-mean-squared differences between water vapor retrievals and dedicated radiosondes vary with height from ~30% near the surface ~12% in the free troposphere beneath the 300 mb surface. RMS differences over land, at the continental margin, and in stratus regions (conditions characterizing three of the four sites considered) are 30-40%.

AIRS total column ozone differs from TOMS globally by -2 to -4 ± 7 %. Average ozone differences against sondes are about -10% in the stratosphere and about +20 to +70% in the troposphere. These biases partially cancel out in evaluating the total column.

Cloud top pressure and its estimated errors for both retrieved pressure levels are compared with the active surface-based measurements located at the Atmospheric Radiation Measurement program site at Manus Island in the Tropical Western Pacific. Good agreement between the upper layer cloud top pressure and the ARM site highest cloud layer is observed for cloud fraction values greater than roughly 0.15. Poorer agreement is seen at lower values of cloud fraction.

Table of Contents

Tables

Figures

1. Introduction

1.1. Overview

This report describes the validation of AIRS/AMSU/HSB retrieved products.
The v3.0 report by Fetzer et al. (2003) addresses radiances, and provides much of the supporting information for this document.

Validation is the comparison between satellite quantities and other data describing the atmosphere. Those other data come from a variety of sources described in later sections. Retrieved products are validated for the following sets of conditions:

- *Non-polar latitudes* (50 South to 50 North).
- *Ocean and Land*

An overview of the validation status of the AIRS data sets is given in the Executive Summary in Section 2 below.

1.2. Quality Flags

Version 4.0 retrievals differ from Version 3 in the inclusion of a set of field- and height-dependent quality flags. In contrast, Version 3.0 had a single quality flag. The flags and their definitions are shown in Table 1. These flags are discussed in more detail in Olsen et al. (2005).

Qual_MW_Only_Temp_Strat	Overall quality flag for MW-Only temperature fields for altitudes above 201 mbar
Qual_MW_Only_Temp_Tropo	Overall quality flag for MW-Only temperature fields for altitudes at and below 201 mbar, including surface temperature.
Qual_MW_Only_H2O	Overall quality flag for MW-Only water (both vapor and liquid) fields. The possible values this flag are 1(H2O retrieval fully valid), 1(only total precipitable water vapor is valid), 2(H2O invalid)
Qual_Cloud_OLR	Overall quality flag for cloud parameters and clear and cloudy OLR
Qual_H2O	Overall quality flag for water vapor fields
Qual_CO	Quality flag for CO
Qual_O3	Quality flag for ozone
Qual_Temp_Profile_Top	Quality flag for temperature profile at and above Press_mid_top_bndry mbar (currently 200 mb)
Qual_Temp_Profile_Mid	Quality flag for temperature profile between Press_mid_top_bndry mbar and Press_bot_mid_bndry mbar (currently 3 km above surface)
Qual_Temp_Profile_Bot	Quality flag for temperature profile below Press_bot_mid_bndry mbar, including surface air temperature

Qual_Surf	Overall quality flag for surface fields including surface temperature, emissivity, and reflectivity
Qual_CC_Rad	Overall quality flag for cloud cleared radiances
Qual_Guess_PSurf	Quality flag for surface pressure guess input. The possible values are 0 (good surface pressure guess from valid forecast), 1 (surface pressure guess estimated from topography), and 2 (do not use)

Table 1. Version 4.0 quality flags.

1.3. Quantities Analyzed for This Report

Table 2 gives an overview of retrieved Cloud Cleared Radiances and Standard Products analyzed for this report. Table 3 describes the current understanding of the error estimates generated by the retrieval algorithm. Table 4 gives the validation status of all other Level 2 Standard Products.

	Correlative Data Sets and Regions of Analyses					
Variable Name	**Model Reanalyses**		**Satellite Data**		**Instrumented Sites (Primarily sondes)**	
	Land	**Ocean**	**Land**	**Ocean**	**Land**	**Ocean**
Cloud-Cleared Radiances		•				
TsurfStd		•		•		
TairStd	•	•			•	•
H2OMMRStd					•	•
totH2OStd			•	•	#	#
O3VMRStd					•	•
totO3Std			•	•		
PCldTopStd					•	•
CldFrcStd					•	•

#: sonde comparisons of total water are integrated from H2OMMRStd

Table 2. Variables examined in this report and correlative data sets used in analyses.

Variable Name	**Correlative Data Source**	**Validation Status**
TsurfStdErr	AMSR-E	Means roughly correct, no scene-dependent skill.
TairStdErr	Sondes	Means roughly correct, no scene-dependent skill.
H2OMMRStdErr	Sondes	Means roughly correct, no scene-dependent skill.
totH2OStdErr	AMSR-E	Means roughly correct, no scene-dependent skill.
PCldTopStdErr	Lidar	Means unknown, possible scene-dependent skill.
CldFrcStdErr	Lidar	Means unknown, possible scene-dependent skill.

Table 3. Validation status of retrieved error estimates.

Variable Name	Validation Status
numCloud	Implicitly validated with PcldTopStd and CldFrcStd.
PsurfStd	Not retrieved. Generated from model reanalyses.
TsurfAir	No validation analyses performed to date.
H2OMMRSat	Implicitly validated with TAirStd.
emisIRStd	No validation analyses performed to date.
rhoIRStd	No validation analyses performed to date.
sfcTbMWStd	No validation analyses performed to date.
EmisMWStd	No validation analyses performed to date.
totCldH2OStd	No validation analyses performed to date.
TCldTopStd	Implicitly validated with TAirStd and PCldTopStd.
CldClearParamStd	No validation analyses performed to date.
PsurfStdErr	No validation analyses performed to date.
totH2OStdErr	No validation analyses performed to date.
O3VMRStdErr	No validation analyses performed to date.
totO3StdErr	No validation analyses performed to date.
emisIRStdErr	No validation analyses performed to date.
rhoIRStdErr	No validation analyses performed to date.
EmisMWStdErr	No validation analyses performed to date.
totCldH2OStdErr	No validation analyses performed to date.
TCldTopStdErr	Implicitly validated with TairStd, TairStdErr, PcldTopStd, PcldTopStdErr.
CldClearParamStdErr	No validation analyses performed to date.
GPHeight	No validation analyses performed to date.
clear_flag_4um	No validation analyses performed to date.
clear_flag_11um	No validation analyses performed to date.
clear_flag	No validation analyses performed to date.

Table 4. Validation status of all other Level 2 Standard Product retrieved quantities.

1.4. Supporting Documents

Two important documents are:

Fetzer, E. J, H. H. Aumann, F. Chen, L. Chen, S. Gaiser, D. Hagan, T. Hearty, F. W. Irion, S.-Y. Lee, L. McMillin, E. Olsen, H. Revercomb, P. Rosenkranz, D. Staelin, L. Strow, J. Susskind, D. Tobin, and J. Zhou. Validation Of AIRS/AMSU/HSB Core Products for Data Release Version 3.0, August 13, 2003, JPL D-26538, 79 pages. Available online at http://daac.gsfc.nasa.gov/atmodyn/airs/.

E. Olsen, H. Aumann, S. Broberg, L. Chen, D. Elliott, E. Fetzer, E. Fishbein, S. Friedman, S. Gaiser, S. Granger, M. Kapoor, B. Lambrigtsen, S.-Y. Lee, S. Licata and E. Manning. AIRS/AMSU/HSB Version 4.0 Data Release User Guide, February 28, 2005, 70 pages.

2. Executive Summary

The following summarizes the results of each section. Details of those analyses are given in each section.

- Section 3.1 *Cloud-Cleared Infrared Radiances*. We show intercomparisons of AIRS retrieved cloud cleared radiances and clear sky radiances calculated from ECMWF global forecasts and analyses over ocean. We consider two carbon dioxide Q-branches at 667.38 and 720.81 cm^{-1}. Biases are greatest in the middle and upper stratosphere (~0.3 K) , and in the lower troposphere near the surface (~0.4 K). Differences in brightness temperature are comparable to difference in profile temperatures between ECMWF fields and radiosondes.
- Section 3.2 *Surface Temperatures*. Retrieved sea surface temperatures are compared with ECMWF, and with AMSR-E on the *Aqua* satellite. These comparisons show a difference of about –0.6 ± 0.9 K, against ECMWF and -0.4 ± 0.8 K against AMSR-E. The yield for the "Highest Quality" SST retrievals (i.e., Qual_Surf = 0 over ocean) against ECMWF in v4.0.0.0 is ~ 12% for ascending nodes (day) and 9% for descending nodes (night). Yield for v3.7.7 retrievals was about four times higher, with a corresponding degradation in RMS differences against AMSR-E data sets of about 0.3 K.
- Section 3.3 *Temperature*. The AIRS temperature retrievals were compared with ECMWF analyses and dedicated radiosondes based on the new Quality Assessment (QA) scheme implemented in v4.0.0.0 of the PGE. The v4.0.0.0 yield for the "Highest Quality" air temperatures above 200 mbar (i.e., Qual_Temp_Profile_Top = 0) is nearly double what it was using retrieval_type = 0 retrievals from v3.7.10.0 of the PGE. This increase in yield was accompanied by a slight increase in the RMS difference with respect to ECMWF above 200 mbar. The increase in yield below 200 mbar was less significant, however, the RMS was similar to that of v3.7.10.0 retrievals with retrieval_type = 0. The yield over land below 800-400 mbar (i.e., Qual_Temp_Profile_Bot = 0) decreased relative to the retrieval_type = 0 retrievals from v3.7.10.0 of the PGE but the RMS difference also decreased.
- Section 3.4 *Total Water Vapor*. AIRS retrieved total water vapor is compared against dedicated sondes, ECMWF and AMSR-E. Greatest consistency is seen against oceanic sondes and the purely oceanic AMSR-E retrievals, with RMS differences of only 5-6%. RMS oceanic differences against ECMWF is ~12 %. Over land, differences are 31-45%, with greatest consistency seen against sondes at the ARM SGP sites. These results suggest that AIRS is meeting its specification of 5% over ocean, and, that AMSR-E and sondes are a better correlative data source than ECMWF. Regions with persistent stratocumulus clouds show consistent, wet biases.
- Section 3.5 *Water Vapor Profiles*. Retrieved water vapor is compared against dedicated radiosondes at four sites. Statistics are compile in 2 km layers, using the most stringent QA (Qual_H2O = 0). Largest biases and RMS differences are seen in the 10130-700 mb layer, with best agreement seen in the 700-500 mb

layer. Oceanic sites are generally biased dry with values as great as -25%; the sole land site is essentially unbiased. The best RMS agreement is seen at the ARM TWP site: from 12 to 28%, beneath the 300 mb surface. Other sites lave larger RMS differences. The ARM SGP land site RMS differences are 31-41%. Larger differences are also seen a the Galapagos (SCR) site. These are likely related to the large, wet biases noted above with total water vapor, since the Galapagos lie in a region of extensive stratocumulus.

- Section 3.6 *Ozone Column and Profiles*. We report comparisons of AIRS ozone column retrievals with co-incident EP-TOMS measurements between 50°S and 50°N using Version 4.0.0 (hereinafter referred to as V4) of the AIRS retrieval algorithm and describe changes in results from Version 3.0.8 (referred to as V3). Using selected "focus days" between September 2002 and December 2004, we find that the average (AIRS - TOMS) / TOMS column difference varies from about -2% to +4% with standard deviations of ~ 7%. Comparisons of ozonesondes with coincident AIRS profile retrievals indicate average (AIRS - Sonde) / Sonde differences of about -10% in the stratosphere and about +20 to +70% in the troposphere. These biases partially cancel out in evaluating the total column.
- Section 3.7 Cloud *Fraction and Top Pressure*. We investigate the accuracy of the Version 4.0 AIRS cloud top pressure (CTP) and CTP errors for both pressure levels using the active surface-based measurements located at the Atmospheric Radiation Measurement (ARM) program site at Manus Island in the Tropical Western Pacific. Good agreement between the upper layer CTP and the ARM site highest cloud layer is observed for cloud fraction values greater than roughly 0.15, and less agreement at lower values of cloud fraction. The quality of the assessment is based on the 1-sigma variability of cloud height at the ARM site for a period of time used to reproduce the scale of the AMSU footprint, and the L2 CTP error estimates. For the lower layer cloud fraction, the agreement from case-to-case is much poorer. However, we present histograms of all AIRS CTP, and compare to histograms of ARM data. We find a peak in lower layer cloud frequency consistent with the ARM data for a small sample set of matchup observations.

3. Retrieved Product Validation

3.1. Cloud-Cleared Infrared Radiances

Cloud-cleared (CC) radiances are an intermediate product representing the clear sky radiances emanating from the transmitting portion of a 3x3 array of AIRS footprints covering an AMSU footprint. Cloud-cleared radiances are not estimated when footprints are completely overcast or cloud amount in adjacent footprints are correlated. We have explored three methods of validation CC radiances: 1) comparisons with clear sky calculated radiances estimated from correlative sources, 2) applications of clear-tests on CC radiances, and 3) intercomparison with observed radiances from smaller footprint radiometers.

Comparison with calculated radiances depends on an accurate radiative transfer forward model and an accurate specification of the surface and atmospheric state sufficient to uniquely perform the forward calculation. In the case of AIRS this means specifying the geophysical state both in the vertical and the surface properties over the 45 km AMSU footprint. Generally the largest error sources in the forward calculation are uncertainty in the surface skin temperature or surface emissivity. We will not validate over land owing to the large uncertainty in both skin temperature and spectral surface emissivity. Over ocean the largest uncertainties are uncertainty in the surface skin temperature, except in water and trace gas-sounding channels where atmospheric composition uncertainty is large. High quality radiosondes and hygrometers are helpful in reducing this problem, but as we will show in this section CC radiance errors in CO_2 temperature sounding channels are sufficiently large, that error in water and trace gas sounding channels do not warrant specialized treatment. In this analysis we will calculate radiances from the ECMWF forecast and analysis products.

Application of clear tests involves applying a test, which is true when a scene is clear. This analysis is simple to perform, but is limited by the precision of the test. We shall discuss this in greater detail.

We will also not discuss comparisons with observed radiances from smaller footprint radiometers, e.g. MODIS, NAST/I and SHIS. This approach uses the smaller footprint of the coincident observation to peer between the clouds and provide an estimate of the radiance from the clear scene, but requires an accurate means to identify clear footprints and assign error estimates to the amount of cloud contamination. We believe the error in the MODIS clear flag is not sufficiently well characterized at this time to be suitable for CC radiance validation. The NAST/I and SHIS under flight data are useful, but are limited in number and are not discussed here.

Figure 1 shows mean and average differences between CC radiances and calculated radiances from granule 176 on 6 September 2002. The largest differences occur in the 4.5 micron CO_2 sounding channels that sound the upper troposphere and stratosphere. These differences arise because of the inability of the radiative transfer forward model to include non-local thermal equilibrium (LTE) processes. The curvature in the difference at wavenumber greater than 2500 cm^{-1} arises from uncertainty in the computed solar reflected radiance from the surface (the reflectivity of the downward solar radiances and thermal radiances are different, but assumed equal). The water sounding

channels (at 1250 – 1650 cm^{-1}) show a reversal between a negative bias in the lower troposphere and a positive bias in the mid to upper troposphere sounding channels – this is similar to the bias in the temperature sounding channels below 750 cm^{-1}. Two likely error sources are cloud contamination and uncertainty in sea-surface skin temperature. To distinguish between these two error sources we examine how the difference varies with sounding height for temperature sounding channels.

Figure 2 shows a sequence of weighting functions from the ν_2 fundamental and combination $\nu_{1,2}$ Q-branches at 667.38 and 720.81 cm^{-1}. Note that only the 721.54 and 723.33 cm^{-1} channels have significant surface emissions. Figure 3 shows the mean AIRS-model brightness temperature difference for all channels. All footprints where cloud clearing was successful are included in the statistics. The difference is plotted versus centroid pressure:

$$P_c = \frac{\int \ln(P) W(P)\, dP}{\int W(P)\, dP}$$

where *W(P)* is the weighting function calculated for the US standard atmosphere over a still ocean viewed in the nadir; the pressure centroids are shown on Figure 2 by the solid triangles. The centroids is always located above the peak of the weighting function and are located above 50 hPa when channels are insensitive to clouds, i.e. the contribution below 100 hPa is less than 5%.

Averages are generated over land (dashed curve) and ocean (solid curve) and the frequencies of the channels are indicated on the ocean curve only (blue is the ν_2 Q-branch and red is the $\nu_{1,2}$ Q-branches). Although the land and ocean curves are different at all levels, the large differences in the upper stratosphere(P < 10 hPa) are surprising because these channels are not cloud-cleared. This difference arises because the ECMWF analysis uses satellite observations differently over land and ocean. There is generally good agreement between the ν_2 and $\nu_{1,2}$ channels in the mid stratosphere except for a –0.1 K bias in the 720.35 and 720.65 cm^{-1} channels at the center of the $\nu_{1,2}$ band; this is an error in the radiative transfer forward model. Lastly there is a uniformly increasing negative bias descending through the troposphere. Although the tropospheric analysis is known to have some biases of the order of 0.1 K at some levels, this, the vertical extend of the bias and dependence on centroid pressure is consistent with an error in cloud clearing.

Version 4 processing has new CC radiance quality control based on the rate of convergence of the cloud-clearing procedure. The parameter, `Qual_CC_Rad,` equals 0 when the CC radiances are of good quality, 1 when they are questionable and 2 where poor. Figure 4 shows the radiance biases plotted against pressure for the good retrievals (green), bad retrievals (red) and all (black). Note that although the mean bias for all footprints is less than 0.1K the good retrievals have a –0.1K bias and the bad retrievals have a +0.3K bias. The negative bias of the good footprints continues to decrease to –0.3K while the bad footprints have greater than –1.0K of bias in the lower troposphere. This indicates that the quality flag has skill identifying poor CC radiances. Figure 5 show our estimate of the cloud cleared radiance bias versus height for all footprints and those indicated good by `Qual_CC_Rad.`

Estimating precision is slightly more difficult. Figure 6 shows a sequence of histograms of radiance differences through the stratosphere and troposphere. The black

curves are differences from all footprints while the green curves are footprints identified with good CC radiances. Panels A and B show stratospheric channels insensitive to clouds. The agreement for channel at 667.78 cm^{-1} located in the core of the ν_2 band is poor because of uncertainty in the model state of the stratosphere and radiative transfer modeling error. The 662.02 cm^{-1} channel shows good agreement that is independent of ***Qual_CC_Rad.*** The next two channels have greater sensitivity to clouds in the mid and upper troposphere with a reduced number of footprints in the wings of the distribution when quality control is applied. Lastly the lower most channel shows a significantly broader distribution and has markedly reduced number of footprints in the wings of the distribution.

Although some of the width is associated with the errors in the cloud cleared radiances, an unknown component of the error arises from uncertainty in the analyzed field. Figure 7 shows global mean and RMS differences between the ECMWF 00Z analysis and radiosondes during January 2005. Both the RMS and mean difference show a large increasing difference near the surface, similar to those seen in the cloud-cleared radiances.

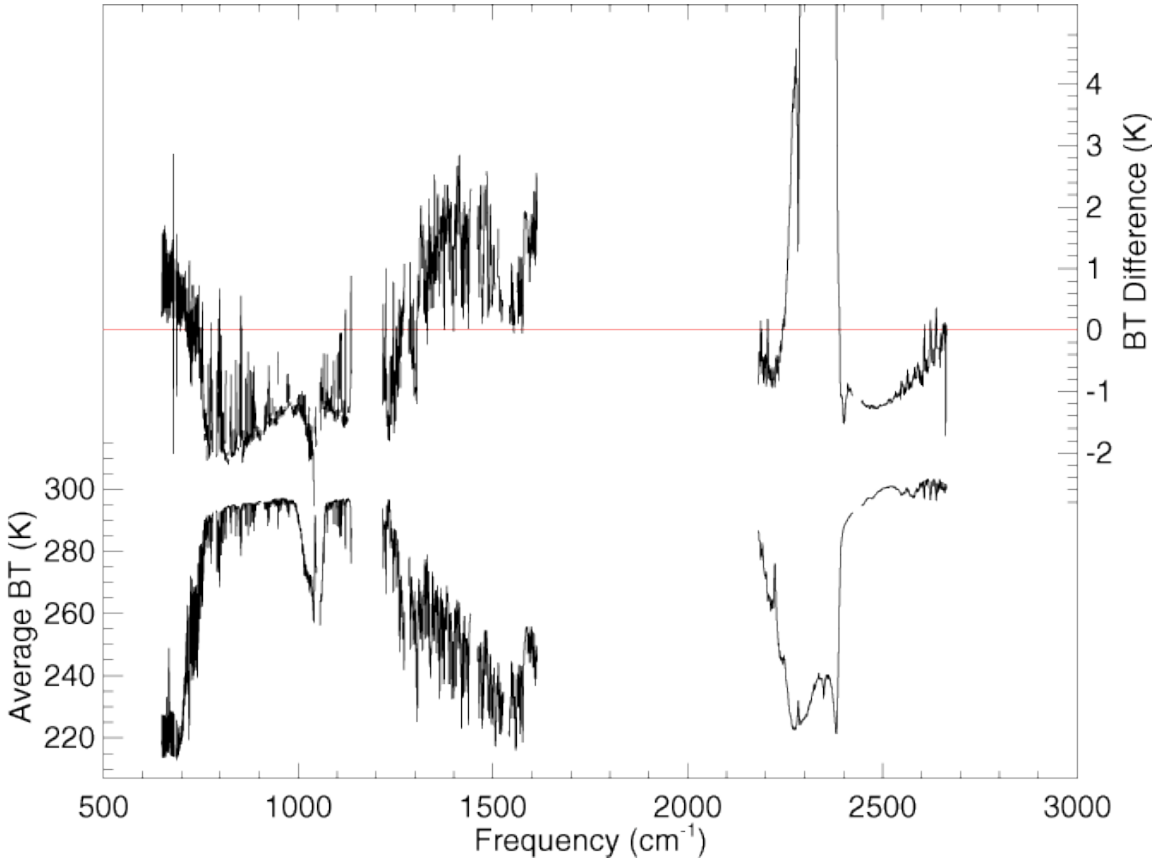

Figure 1. Mean and average differences between CC radiances and calculated radiances from granule 176 on 6 September 2002

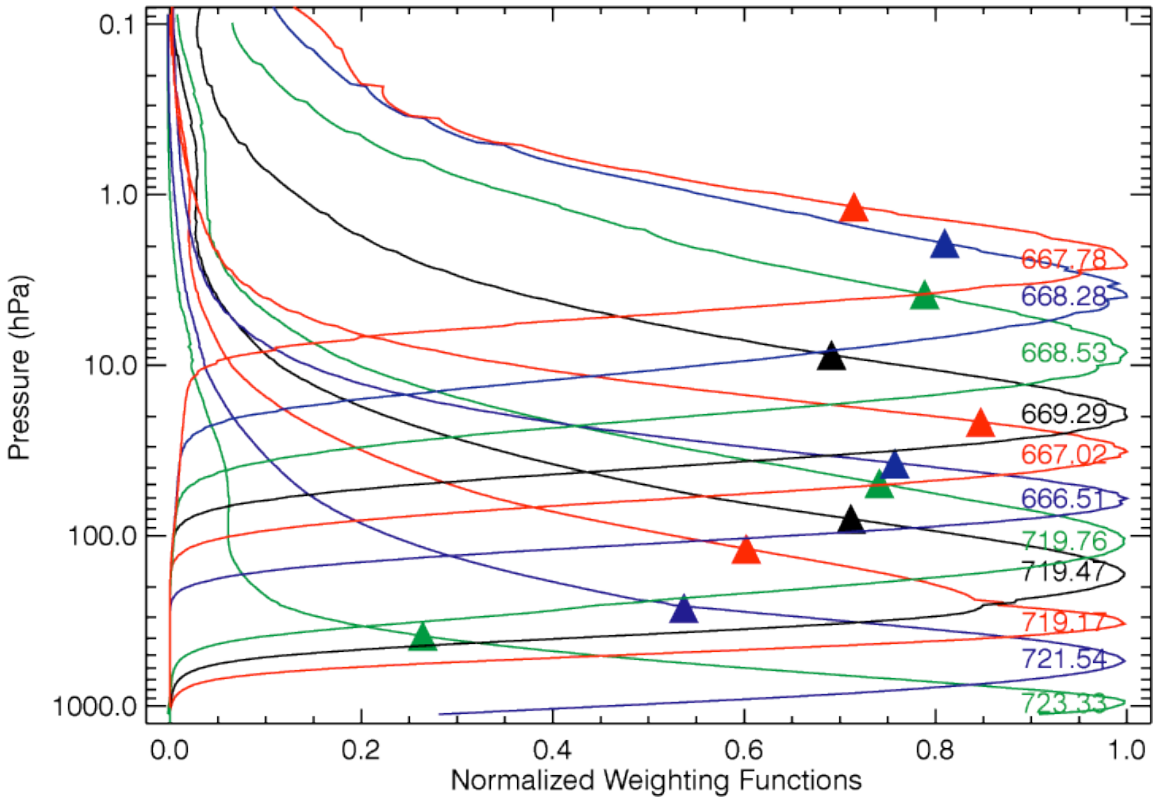

Figure 2. Sequence of weighting functions from the ν_2 fundamental and combination $\nu_{1,2}$ Q-branches at 667.38 and 720.81 cm^{-1}.

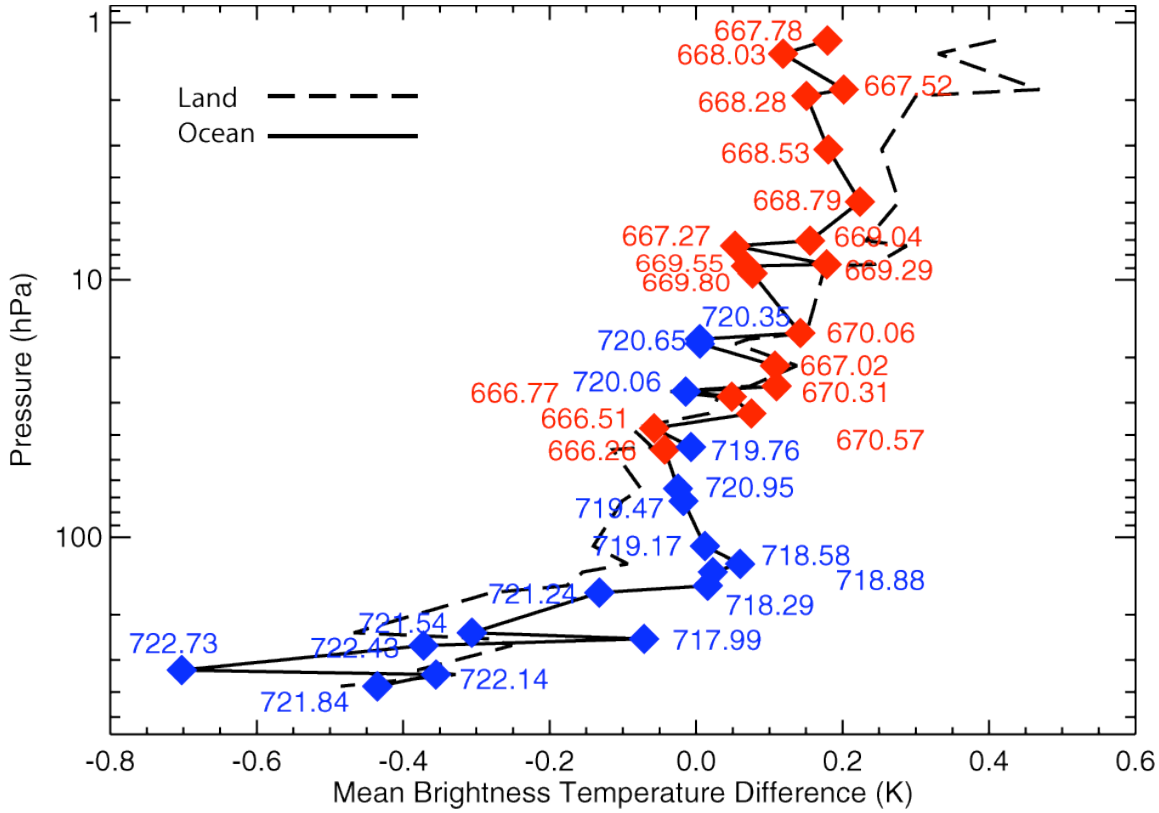

Figure 3. Mean brightness temperature difference for all channels.

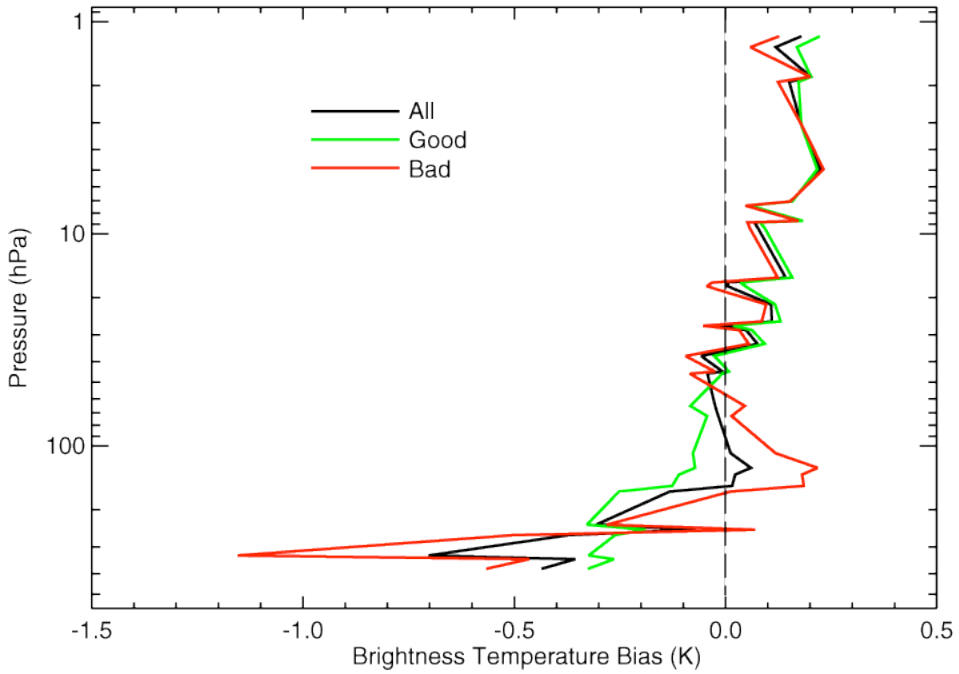

Figure 4. Radiance biases plotted against pressure for good (green), bad (red) and all retrievals (black).

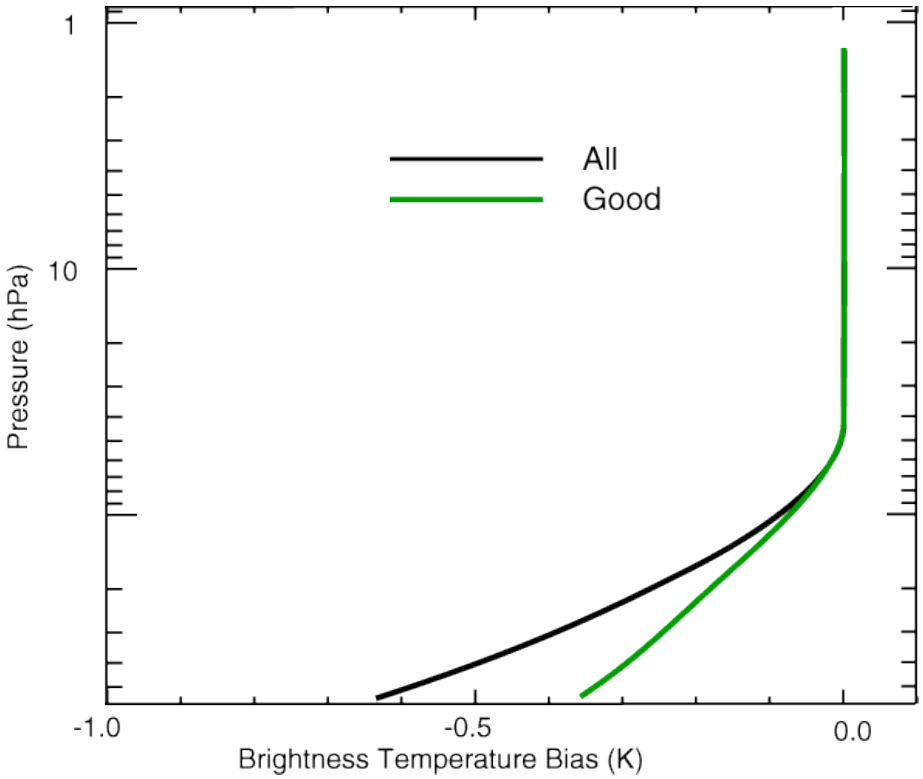

Figure 5. Cloud cleared radiance bias versus height for all footprints and those indicated good by *Qual_CC_Rad*

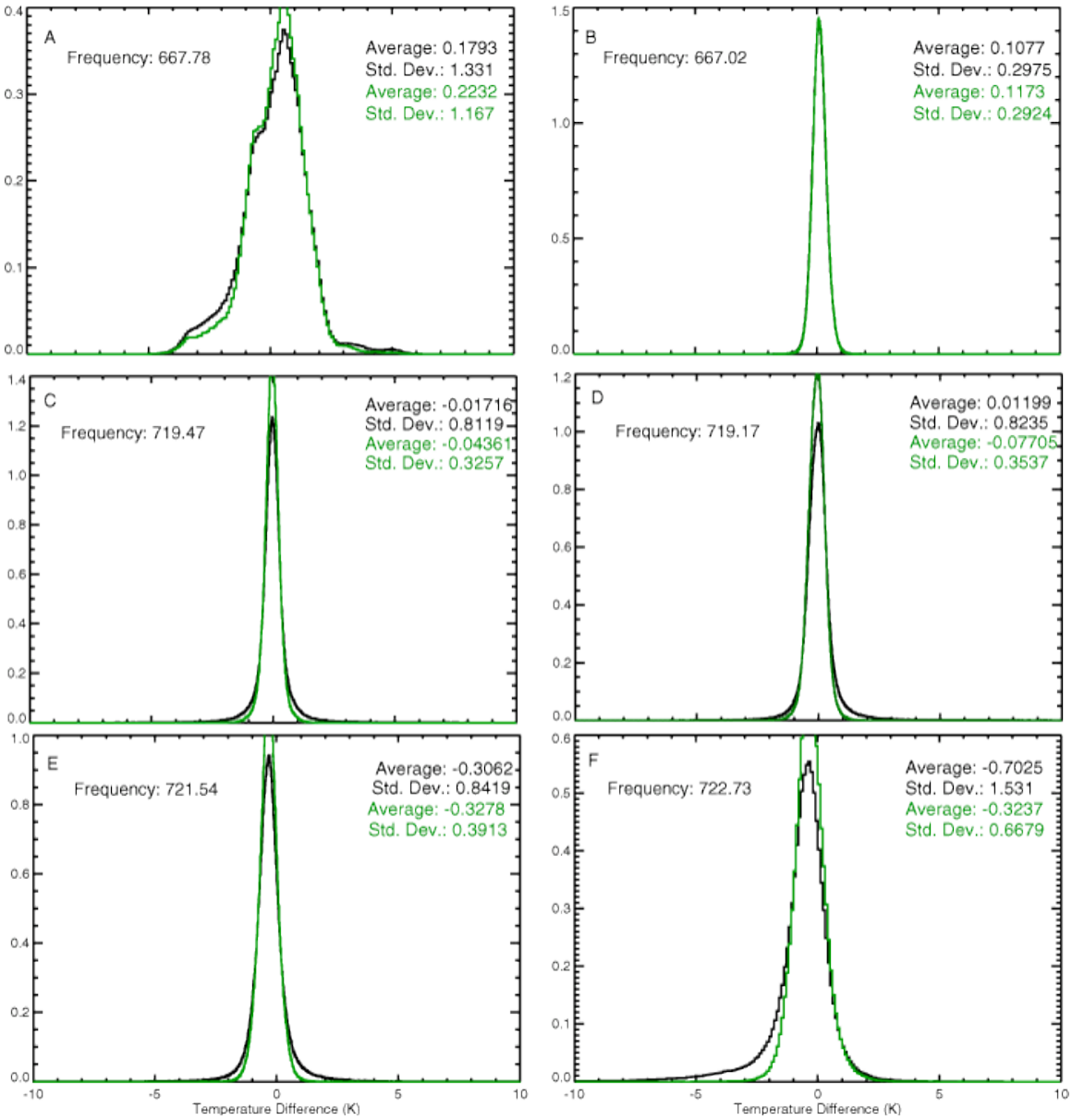

Figure 6. Radiance differences through the stratosphere and troposphere.

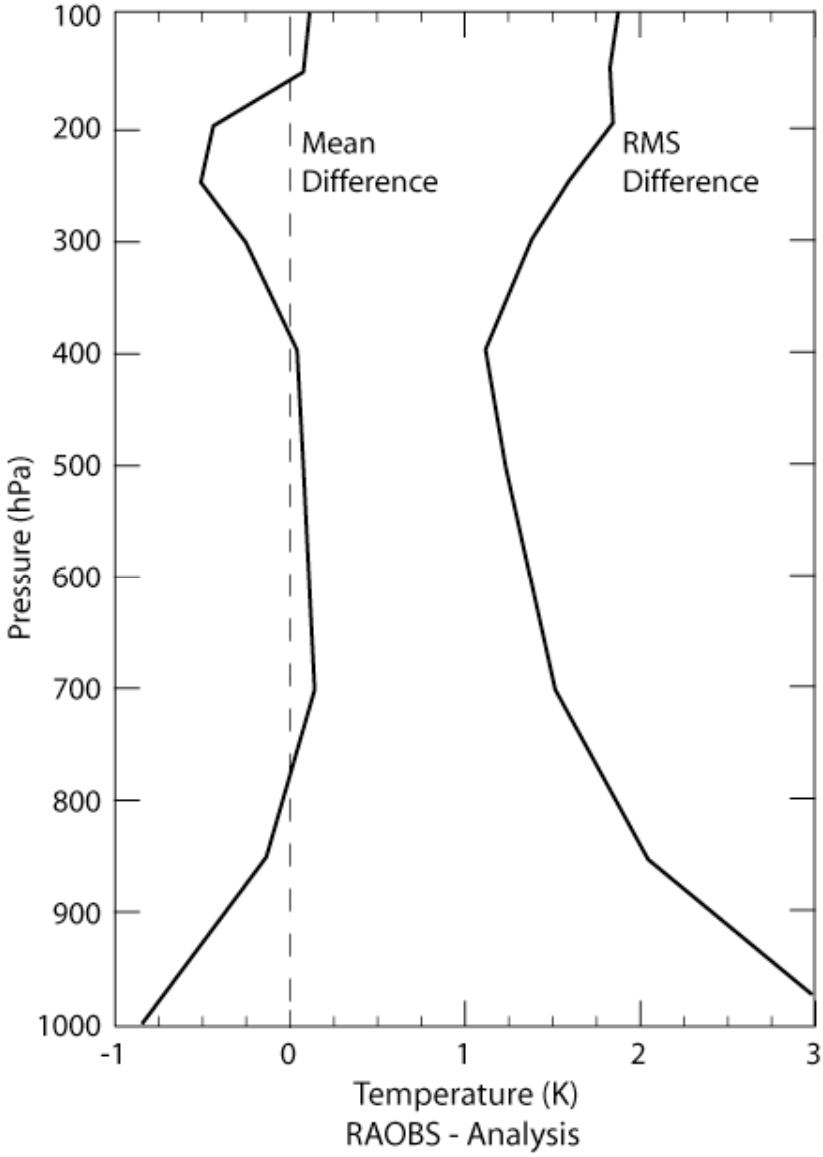

Figure 7. Global mean and rms differences between the ECMWF 00Z analysis and radiosondes during January 2005.

3.2. Surface Temperature

Table 5 summarizes the results of comparisons between AIRS SST and ECMWF and AMSR-E.

Data source	Difference
ECMWF 50S to 50 N	
Ocean night	-0.7 ± 0.8 K
Ocean day	-0.4 ± 0.9 K
AMSR-E 50S to 50 N	
Ocean night (descending orbits)	-0.4 ± 1.0 K
Ocean day (ascending orbits)	-0.3 ± 0.7 K

Table 5. SST differences against ECMWF and AMSR-E.

3.2.1. Comparison with Model Skin Temperature Analyses

Figure 8 shows the global distribution of Qual_Surf (see Table 1) for surface temperature retrievals. Note that all land retrievals have Qual_Surf > 0.

Day and nights maps of the SST differences between retrievals and ECMWF for 6 September 2002 for the retrievals with Qual_Surf = 0 are not shown since they represent only 7.4% of all fields of view. The associated distributions are shown in Figure 9. Statistical summaries are included in that figure.

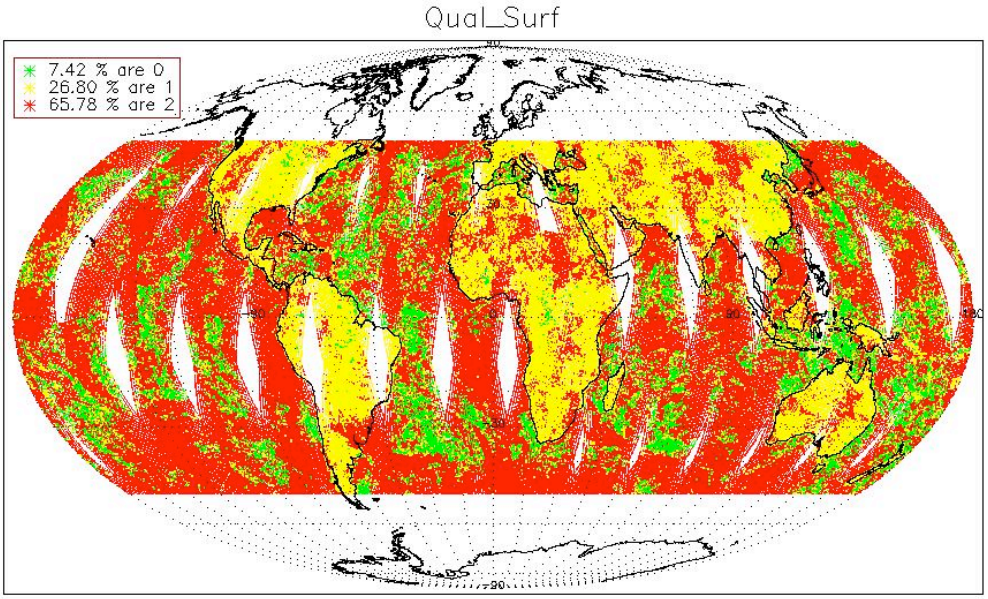

Figure 8. The global distribution of Qual_Surf.

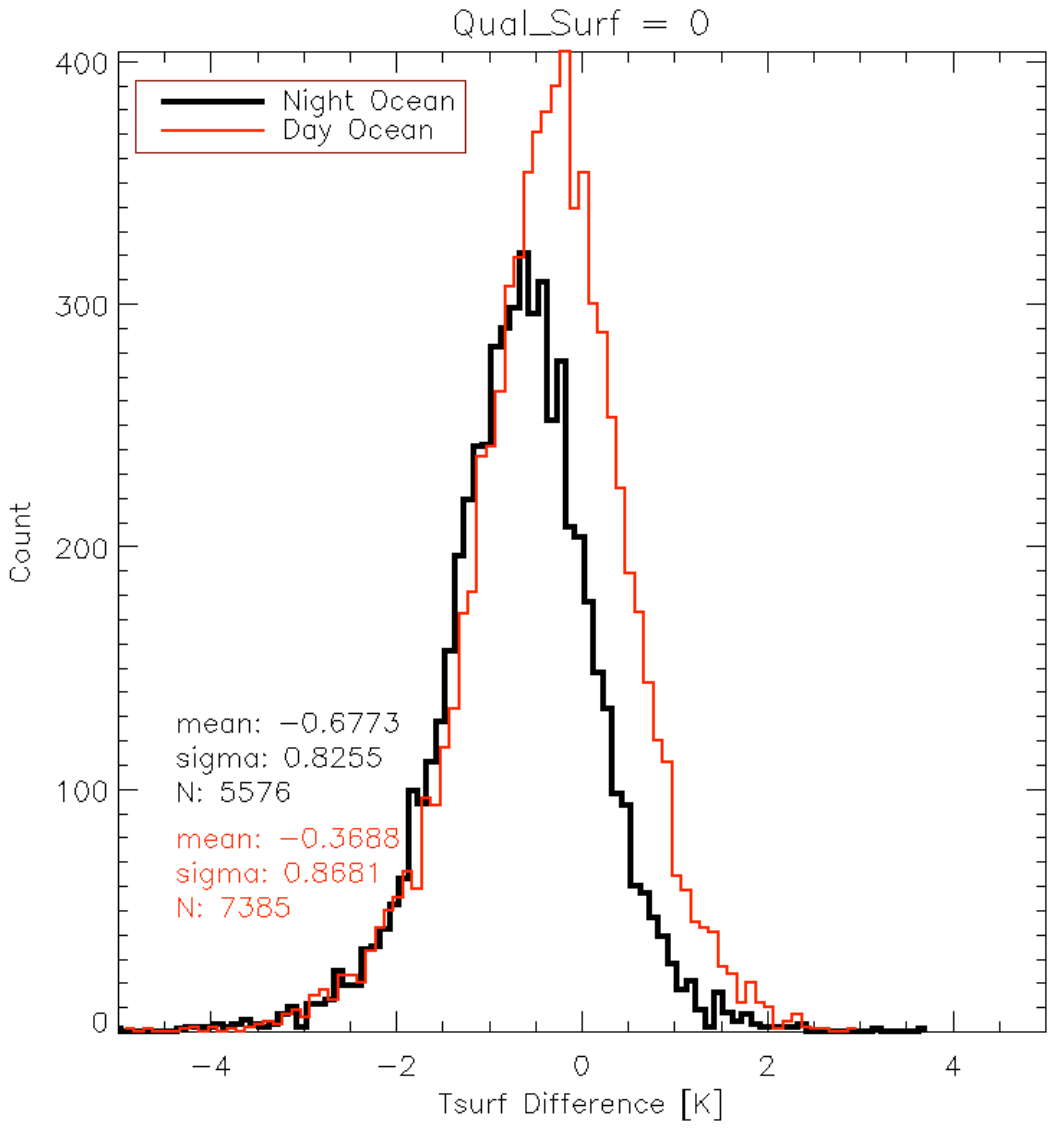

Figure 9. Distribution of differences between the AIRS retrieved Sea Surface Temperature and ECMWF for Qual_Surf = 0.

3.2.2. Comparison with AMSR-E SST

The Advanced Microwave Scanning Radiometer – EOS (AMSR-E) is a companion instrument on *Aqua* measuring both SST and total water vapor, using an independent microwave-only technique. AMSR-E can be treated as an independent validation data source. Here we describe a comparison of AIRS and AMSR-E SST measurement.

In the following comparisons, we consider the nearest 0.25 degree gridded AMSR-E value to an AMSU location; no interpolation is used. Because the instruments are on the same platform the observations are effectively simultaneous. The statistics shown describe global comparisons; later analyses will confine the regions of interest.

Figure 10 shows the differences for ascending orbits of 6 September 2002 for Qual_Surf = 0. Yield is about 5700 matches, compared to roughly 35,0000 matches for Qual_Surf = 1 and 2. Figure 11 shows the analogous graphs for retrieval version 3.7.7. The V3.7.7 yield is four times higher than V4.0, but the root-mean-square differences increases from only 0.78 K to 1.1 K.

Similar results hold for the descending node on 6 September 2002. Below we show the effect of cloud fraction on retrieval of total water vapor.

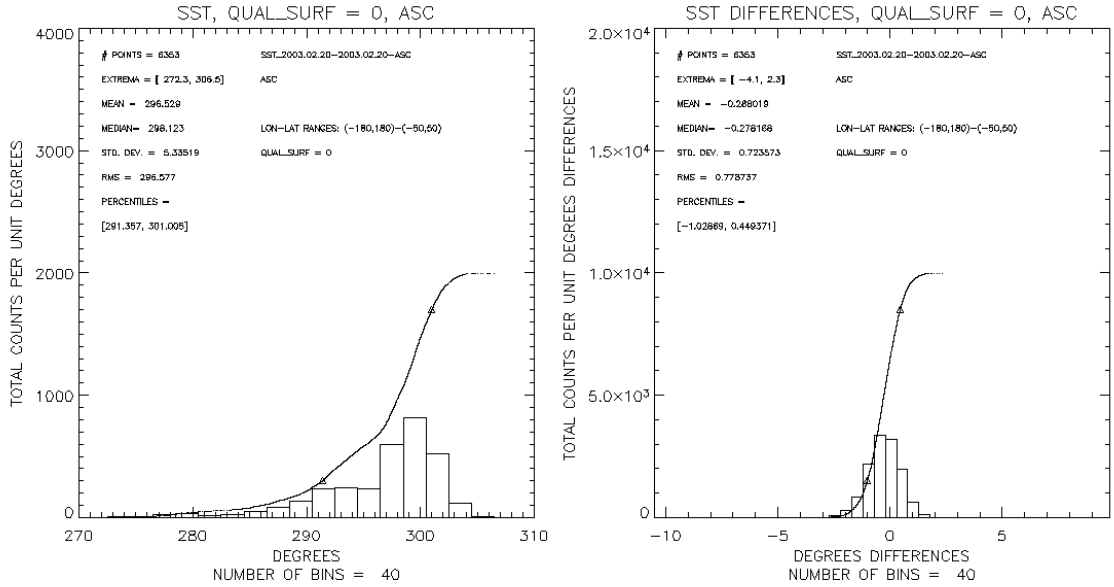

Figure 10. Histogram of AIRS SST values for Qual_Surf = 0 (left) and histogram of AIRS-AMSR-E differences, ascending orbits on 6 September 2002.

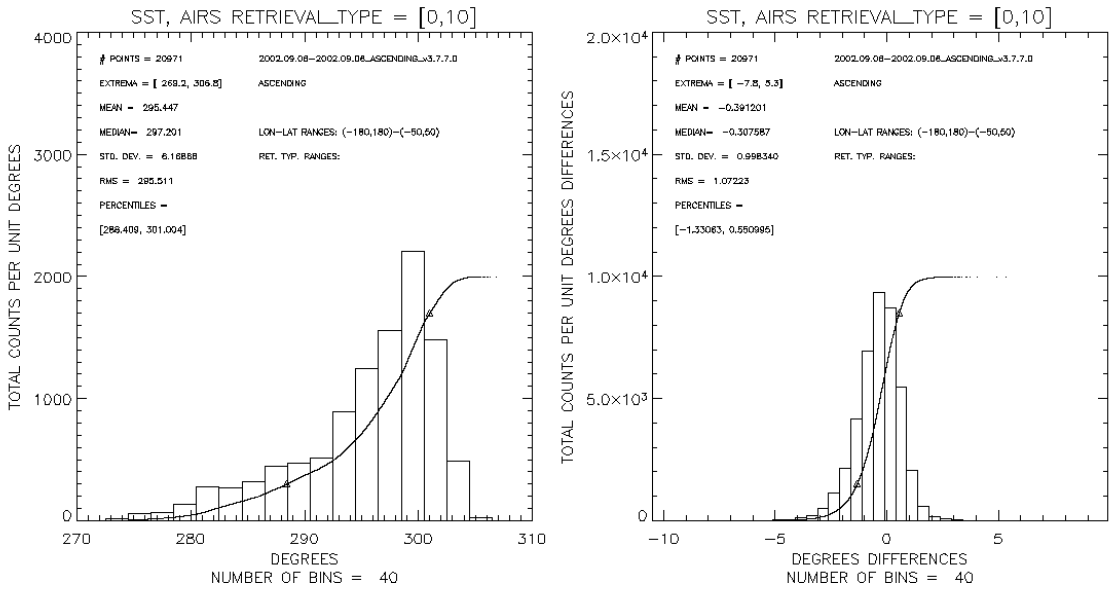

Figure 11. Histogram of AIRS SST values for retrieval_type = 0 (left) and histogram of AIRS-AMSR-E differences, ascending orbits on 6 September 2002.

3.3. Temperature Profiles

Table 6 summarizes the comparisons between AIRS retrieved temperature profiles and correlative data sources.

Data source	Mean Difference Surface-100 mb	RMS Difference, Surface-100 mb	Relevant Figure(s)
ECMWF 50S to 50 N			
Ocean	~±0.5 K	0.7 - 1.2 K	Figure 13, Figure 14
Land	-0.5 – 1.5 K	0.7 – 2.0 K	Figure 15, Figure 16
Dedicated ARM sondes			
TWP	-0.8 – 0.8 K	0.7 – 1.3 K	Figure 18
SGP	-0.1 – 0.9 K	1.0 – 1.8 K	Figure 19

Table 6. Summary of differences between AIRS retrieved temperature profiles and ECMWF and radiosondes.

3.3.1. Comparison with Model Reanalyses

This section describes comparisons between AIRS temperature retrievals and ECMWF analyses. The comparisons are made by averaging both fields over 1 km thick layers, differencing the averages, then, compiling statistics on the differences. Fishbein et al., 2003, describes the method for interpolating the synoptic ECMWF to the location of the AIRS/AMSU/HSB observations. The new QA scheme allows retrievals to be valid in higher layers when they are invalid in lower layers. Figure 12 shows the global distribution of data for Qual_Temp_Proflile_Top, Qual_Temp_Profile_Mid, and Qual_Temp_Profile_Bot. Figure 13 shows the temperature bias and RMS with these flags set to zero over the ocean for 14 "Focus Days." The figures also show the bias, RMS, and yield for Focus Day 3 from v3.7.10.0 based on retrieval_type = 0. The yield for V4.0 has increase significantly in the upper layer of the atmosphere relative to V3.7.10, with little change in the bias and RMS.

Figure 15 and Figure 16 show the analogous result for land cases.

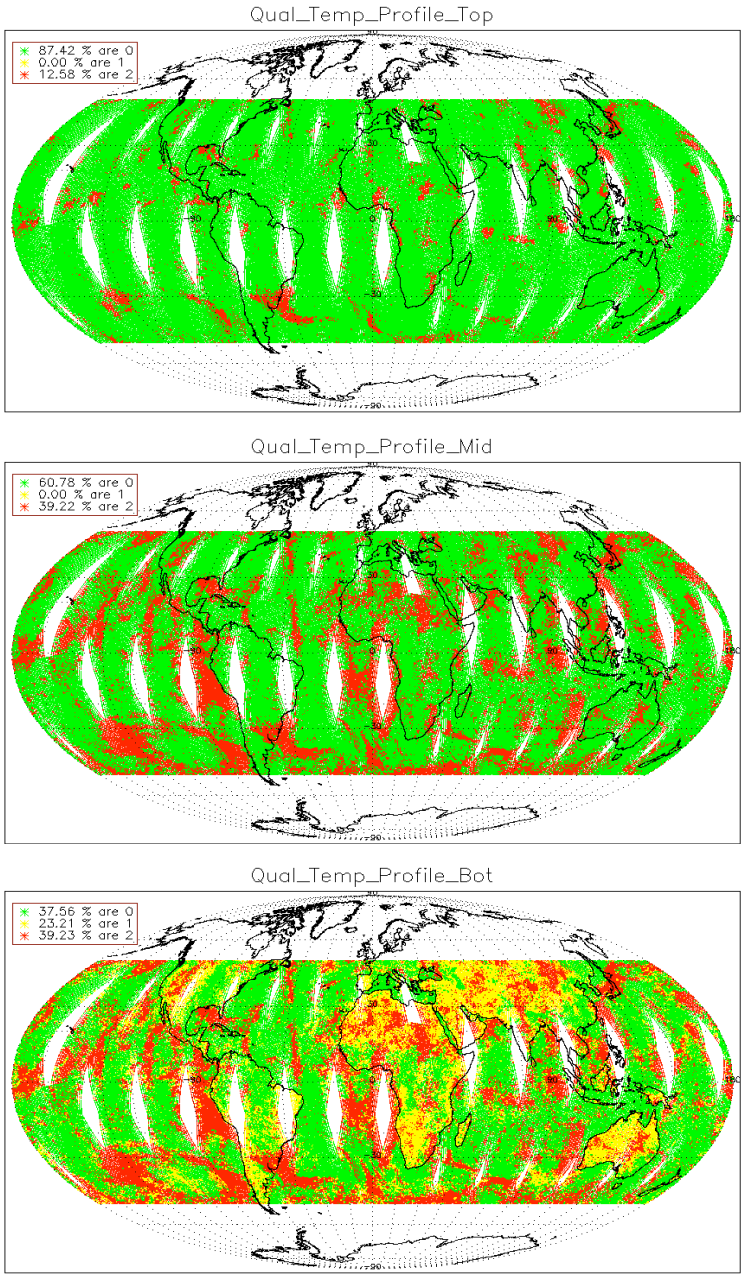

Figure 12. Spatial distribution of Qual_Temp_Profile_Bot (upper panel), Qual_Temp_Profile_Mid (middle panel), and Qual_Temp_Profile_Top (bottom panel).

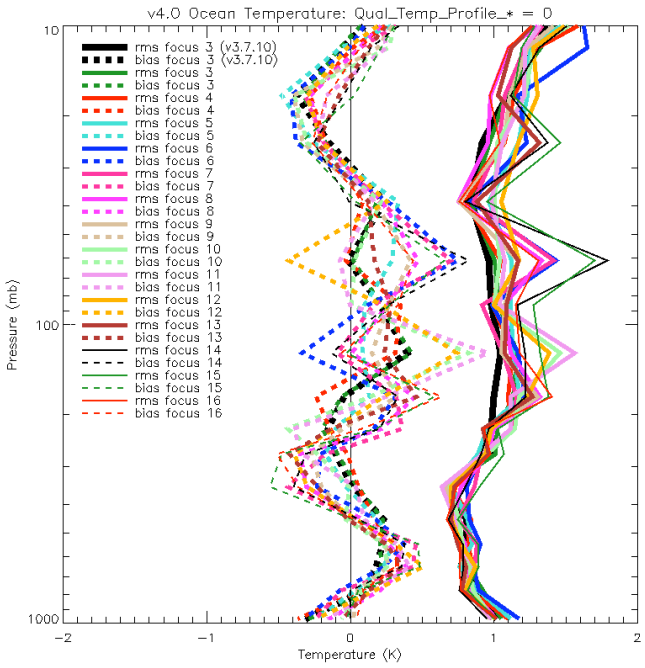

Figure 13. Retrieved air temperature (TAir) bias and RMS over ocean relative to ECMWF. The thick black line shows the bias and RMS for retrieval_type = 0 for Version 3.7.10 retrievals.

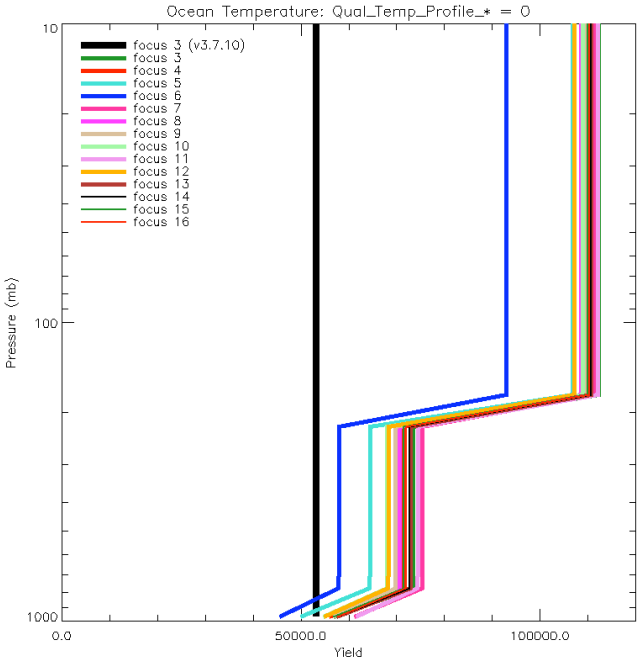

Figure 14. Yield over ocean with Qual_Temp_Profile_Bot, Qual_Temp_Profile_Mid, and Qual_Temp_Profile_Top set to zero. The thick black line shows the yield for retrieval_type = 0 for Version 3.7.10 retrievals.

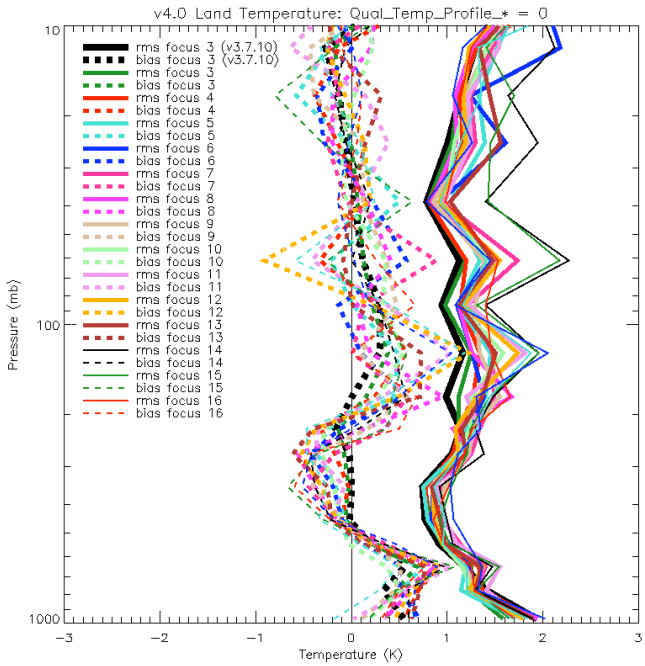

Figure 15. As Figure 13, but over land.

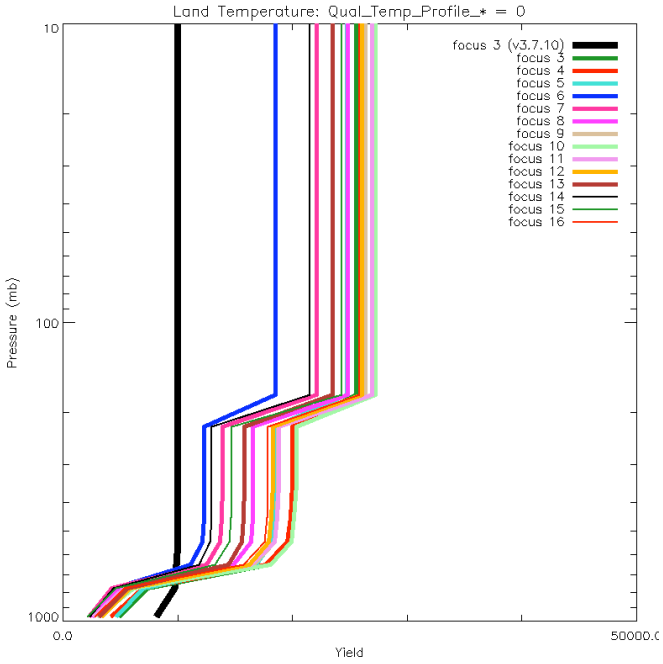

Figure 16. As Figure 14, but over land.

3.3.2. Comparison with Dedicated Radiosondes

Dedicated sondes were analyzed for four locations, the Chesapeake lighthouse platform (CHE), San Cristobal (SCR), Southern Great Plains ARM site (SGP), and the Tropical Western Pacific ARM site (TWP). The SGP is a site over land, while the other sites discussed here are oceanic. Vaisala RS90 and RS80 sondes were used at all sites except SCR. The SCR measurements were made with a combination of Vaisala and frost point hygrometer instruments.

The sonde date were quality checked and then AIRS measurement that were the closest match in space and within 3000 seconds (50 minutes) were selected. The results reported below use the V4.0 quality flags, and for data with a quality flag of zero. When discussing the V4.0 performance relative to v3.5, we are referring to v3.5 data that have retrievals types of 0 and 10.

Figure 17 through Figure 20 below show the vertical profiles of temperature and the bias, RMS, and standard deviation of the AIRS and sonde data for CHE, TWP, SGP , and SCR, respectively.

At CHE, the temperature bias is less than ±1 K at altitudes from the surface up to 20 mb. From the 825 to 70 mb, the bias is less than ± 0.5 K. The RMS differences are between 1.5 and 2.5 K for the whole profile. The AIRS – sonde comparisons shown here are very similar to those for V3.5 retrievals. At TWP, the bias is also smaller than ±1K for all layers from the surface to 20 mb. The RMS differences are less than 1.5K from the surface to 150 mb, and near 2K at pressures less than 150 mb. The RMS difference in the 1000 to 250 mb region as been reduced in v4.0 relative to v3.5 data. At SGP, the temperature bias ranges from 0.5 to –0.8K from the surface to 100 mb. The RMS at SGP ranges from 0.7 to 1.8K from the surface to 200 mb. There is tremendous variability at this location over the time period considered (1 September 2002 to 15 February 2003). The SCR sonde data shows statistics similar to the other locations. The temperature bias is less than ± 0.6K from the surface to 200 mb, and less than ± 1K from the surface to 20 mb. The RMS is less than 1 K from the surface to 150 mb, and grows larger at lower pressures, where the standard deviation of the differences also grows larger.

At TWP and SGP one clearly sees the changes in data yield due to the new quality flags. Version 3.5 and version 4.0 have different number of matchups, and the V4.0 creates vertically dependent number of cases, with TWP using 65 cases in V3.5, and in version 4 there are 40 cases at midtropospheric altitudes and 30 cases in layers near the surface. SGP has a more drastic reduction in data near the surface, changing from 165 cases in V3.5 to 130 cases in v4.0 at mid-troposphere, decreasing to 32 cases in the boundary layer.

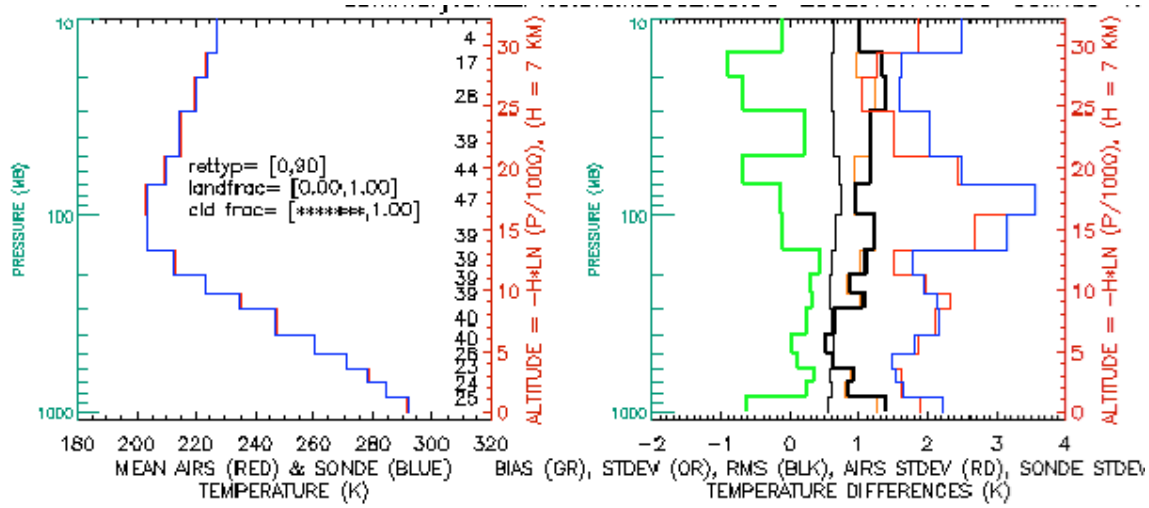

Figure 17. CHE temperature profile

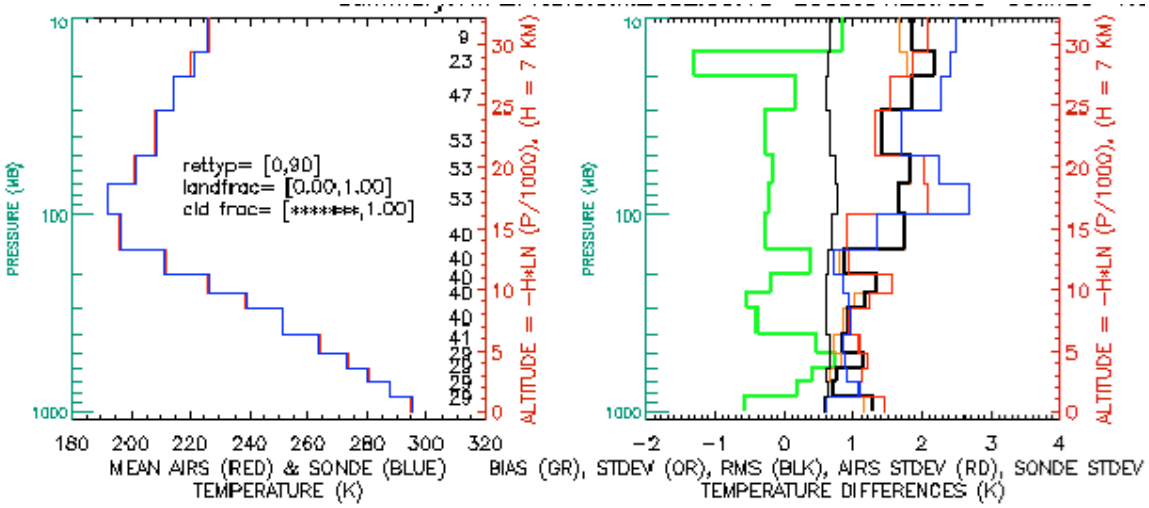

Figure 18. TWP temperature profile

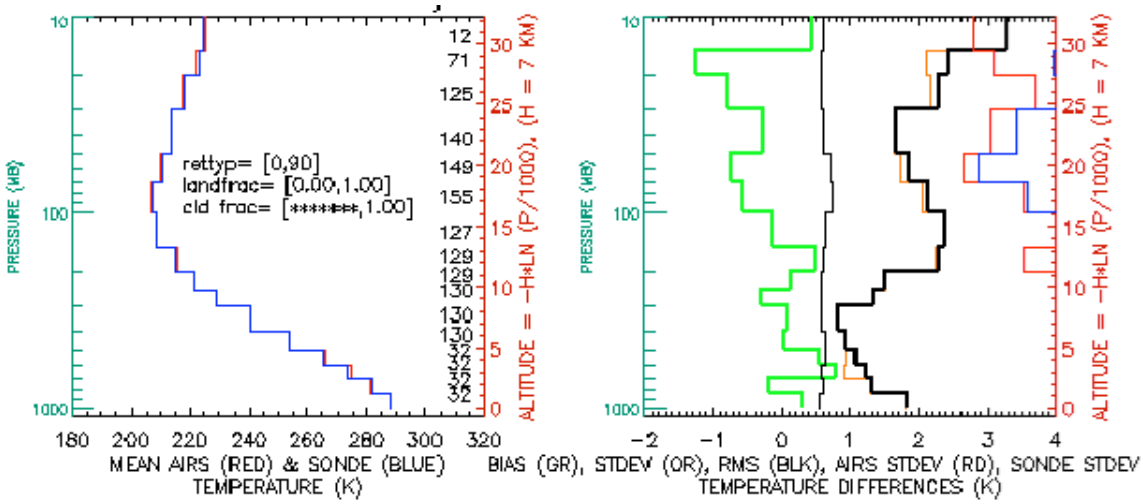

Figure 19. SGP Temperature profiles

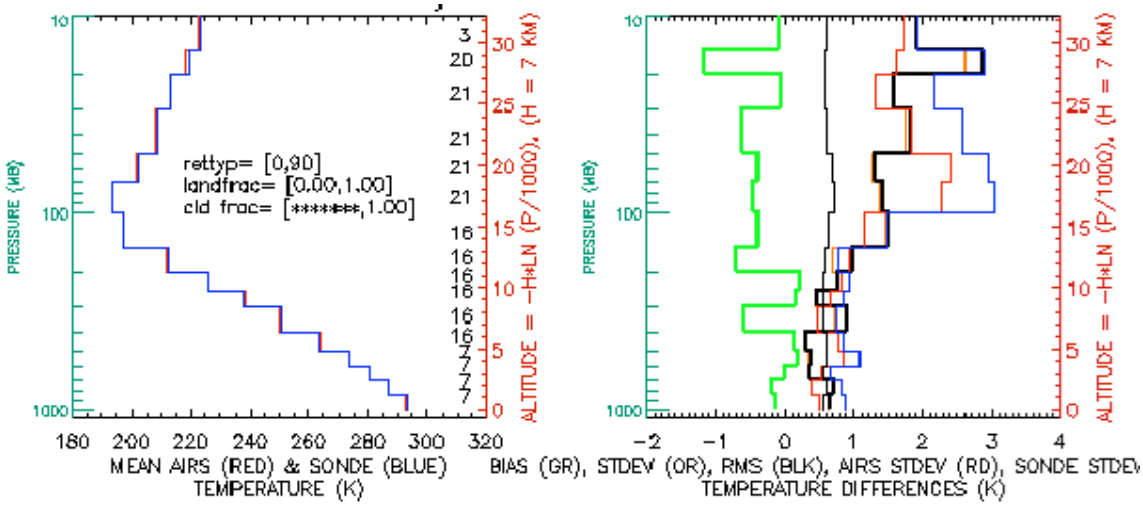

Figure 20. SCR Temperature profiles

3.4. Total Water Vapor

Table 7 summarizes the results of validation analyses for total water vapor.

Data source	Difference	Difference Relative to AIRS Mean	RMS Difference
ECMWF 50S to 50 N			
Ocean night	1.4 ± 3.1 mm	4 ± 11 %	12 %
Ocean day	0.8 ± 3.2 mm	2 ± 12 %	12 %
Land night	0.9 ± 5.3 mm	-1 ± 36 %	36 %
Land day	2.3 ± 5.4 mm	5 ± 43 %	43 %
AMSR-E 50S to 50 N			
Ocean night	0.6 ± 1.5 mm	2 ± 5 %	5 %
Ocean day	-0.1 ± 1.8 mm	0 ± 6 %	6 %
Dedicated ARM sondes			
TWP	0.3 ± 2.9 mm	1 ± 6	6 %
SGP	4.4 ± 3.5 mm	24 ± 19	31 %

Table 7. Bias and, standard deviations and RMS absolute and relative differences in total water vapor for three data sources. ECMWF and AMSR-E are for 6 September 2002.

3.4.1. Comparison with Model Analyses

The distribution of absolute differences between AIRS retrieved and ECMWF total water vapor for 6 September 2003 is shown in Figure 21. The distribution of percent differences is shown in Figure 22. The statistics of the differences are summarized in Table 7.

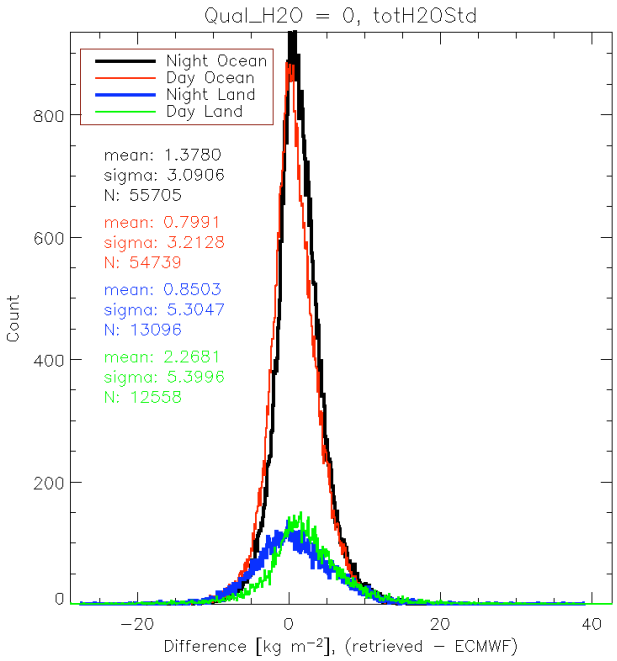

Figure 21. Distribution of difference of the total precipitable water (totH2Ostd) with respect to ECMWF. The night, day, land, ocean case statistical summaries for ±50º latitude are shown.

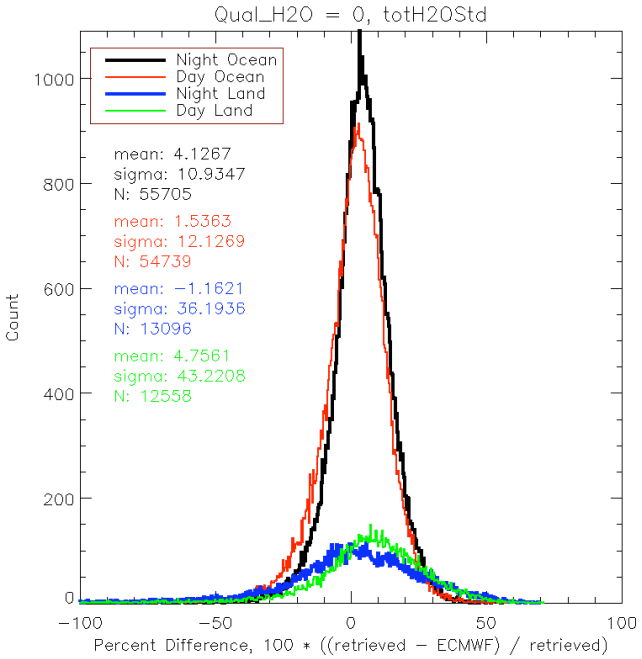

Figure 22. As previous figure, but for percent differences.

3.4.2. Comparison with Dedicated Radiosondes

We show here comparisons with dedicated radiosondes at the ARM Tropical Western Pacific (TWP) and Southern Great Plains (SGP) sites. These represent moist tropical and midlatitude continental conditions, respectively. Figure 23 shows the comparison of AIRS and sonde total water vapor measurements at ARM TWP. The RMS difference is 5.6% relative to the time mean AIRS, and the bias is 0.6%.

Figure 24 is the comparison of AIRS versus radiosonde total water vapor at SGP over two seasons. At SGP the RMS difference is 9.5%, dominated by a mean difference of 7.5%. The result at SGP holds for the winter and fall seasons separately; the points nearer the origin on the plot are from wintertime.

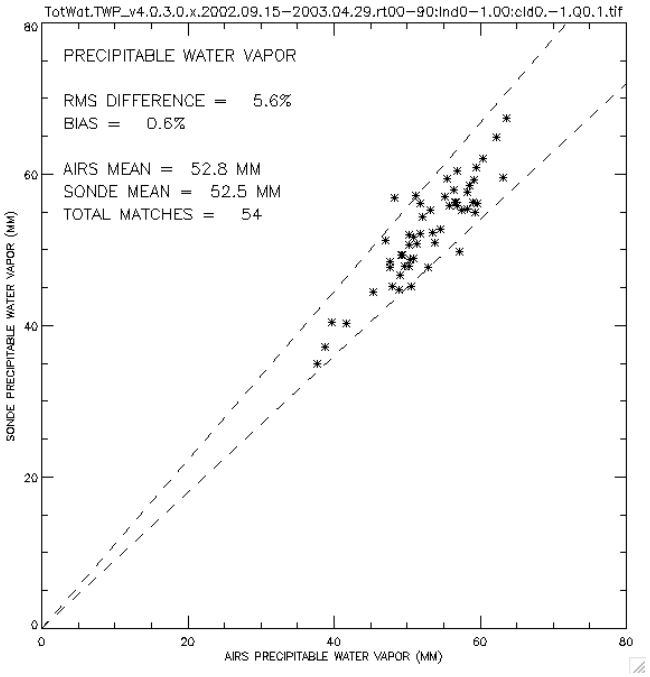

Figure 23. AIRS retrieved versus radiosonde measured total water vapor at ARM TWP site for the period 15 September 2002 to 29 April 2003. Dashed lines show ±5% variability.

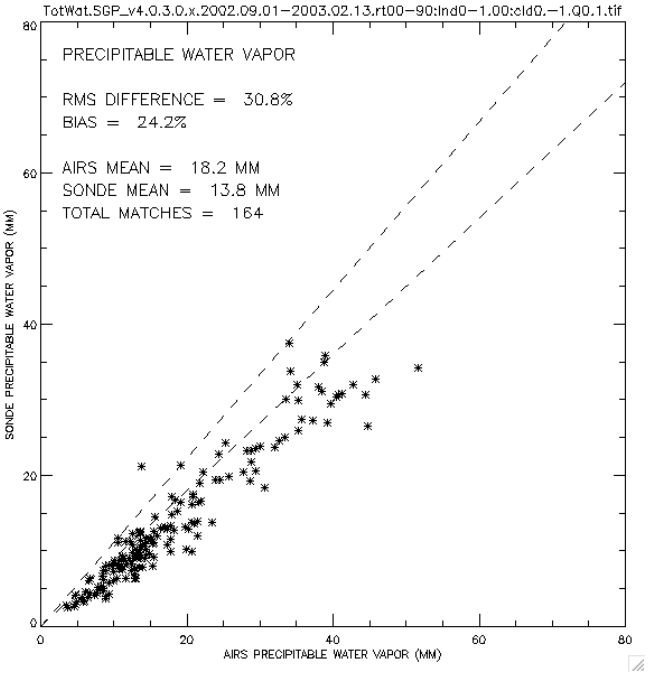

Figure 24. AIRS retrieved versus radiosonde measured total water vapor at ARM SGP site for the period 9 September 2002 to 22 March 2003.

3.4.3. Comparison with AMSR-E

In Section 3.2.2 we described a comparison of AIRS and AMSR-E retrieved SST. Here we compare AIRS and AMSR-E total water vapor. Comparisons are confined to Qual_H2O = 0 only.

Figure 25 shows the distribution of AIRS retrieved total water vapor, and its difference with AMSR-E, for descending (nighttime) orbits on 6 September 2002. The mean difference is 0.58 ± 1.50 mm or 51437 points. The mean difference for ascending orbits (not shown) is –0.06 ± 1.77 mm in 51034 points.

Figure 26 shows the locations of extrema during the descending orbits on 6 September 2002. Note the areas of high water vapor (in red) off the west coasts of South America and Africa. This is a well-recognized AIRS retrieval anomaly commonly seen in the presence of stratocumulus cloud cover.

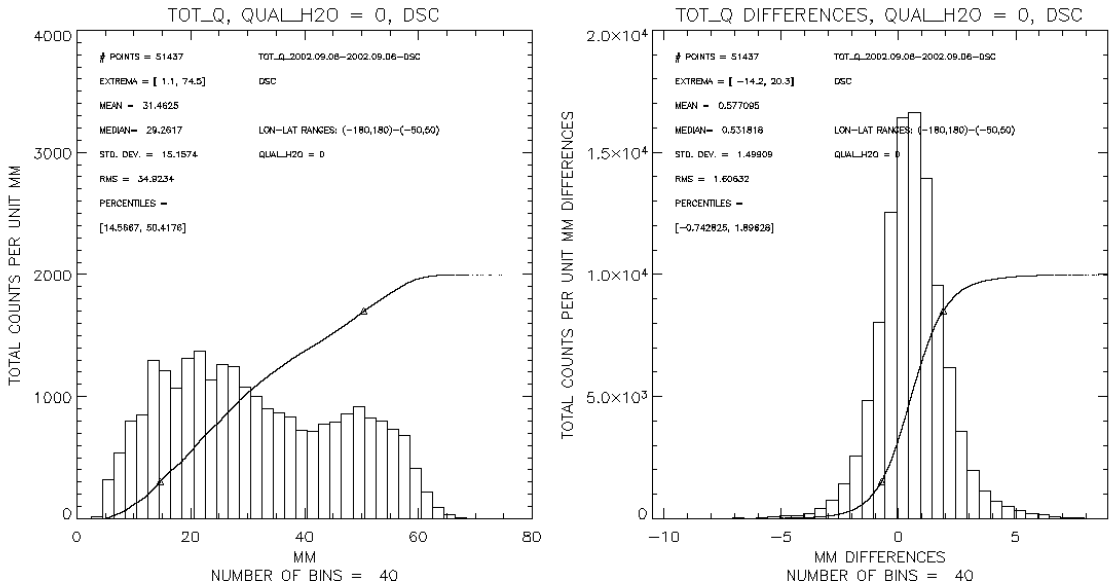

Figure 25. Left: Distribution of AIRS retrieved total water vapor over oceans between 50 S and 50 N, in mm. Right: distribution of AIRS-AMSR-E differences. Mean difference is 0.58 ± 1.50 mm, or 1.8 ± 4.8% relative to AIRS mean.

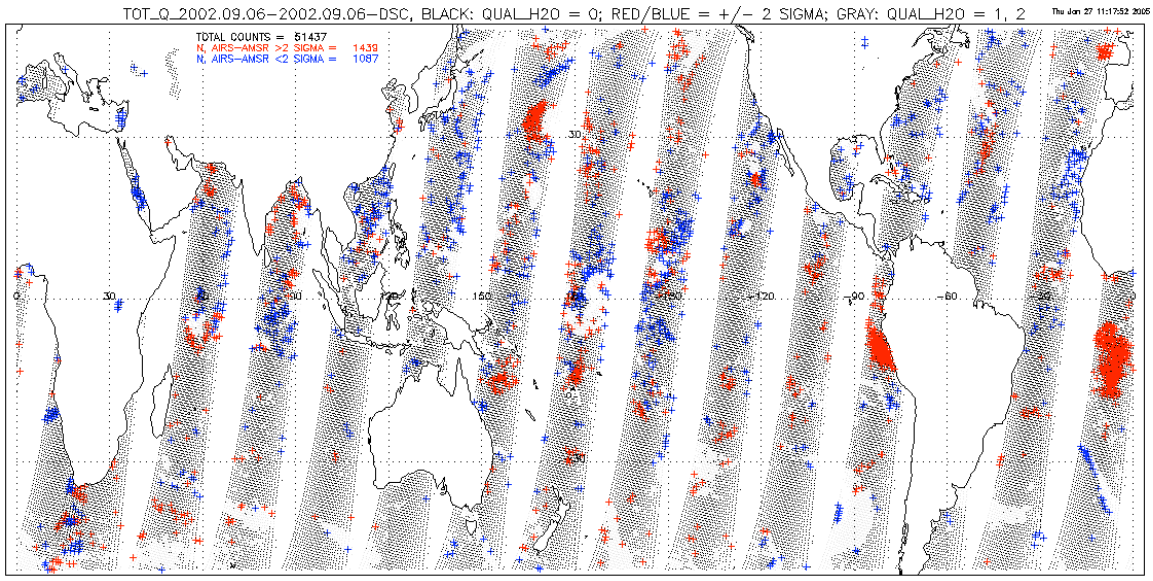

Figure 26. Locations of AIRS retrieved total water vapor drier (blue) and wetter) than AMSR-E by greater than two standard deviations.

3.5. Water Vapor Profiles

3.5.1. Comparison with Dedicated Radiosondes

As with the temperature profiles comparisons in Section 3.3.2, we show comparisons of AIRS retrievals against data from sondes launched from four locations, CHE, TWP, SGP, and SCR. (See that section for definitions of names.) These analyses will be presented for the retrieved water vapor on the AIRS standard product grid with about 1 km vertical resolution, as well as data where the vertical resolution has been averaged to 2 km.

layer	CHE bias	TWP bias	SGP bias	SCR bias
1013-700 mb	-25.1%	-10.5%	0.5%	-18.1%
700-500 mb	12.8%	-0.7%	2.1%	4.2%
500-300 mb	6.7%	-2.3%	-4.3%	9.5%
300-200 mb	4.3%	-16.1%	0.2%	-7.3%
200-150 mb	3.2%	-15.1%	-11.1%	15.5%

Table 8. Biases against sondes for the four launch locations, in 2 km layers.

layer	CHE RMS	TWP RMS	SGP RMS	SCR RMS
1013-700 mb	51.0%	27.5%	41.1%	51.0%
700-500 mb	23.4%	11.7%	24.5%	23.4%
500-300 mb	31.2%	14.8%	31.3%	31.2%
300-200 mb	30.1%	26.5%	36.2%	30.1%

Table 9. RMS differences against sondes for the four launch locations, in 2 km layers.

As seen in these Tables and Figure 27 through Figure 30 the data all meets the specification of 20% accuracy on 2 km layers. The sonde measurements begin to lose sensitivity at pressure levels between 300 and 200 mb, depending on the water vapor concentration. (Gettelman et al. 2004 showed a loss of sensitivity by AIRS at mixing ratios near 10-20 ppmv.)

To portray the underlying data for the water vapor comparison, Figure 31 through Figure 34 below show scatter plots of the water vapor data as well as histograms of the differences. These are presented only for SGP and TWP, which have larger sample sizes and include a land and oceanic site. These figures show that the differences are distributed nearly normally for SGP, where there are nearly 150 samples. Generally, the larger differences occur at the lower water vapor concentrations for a given layer.

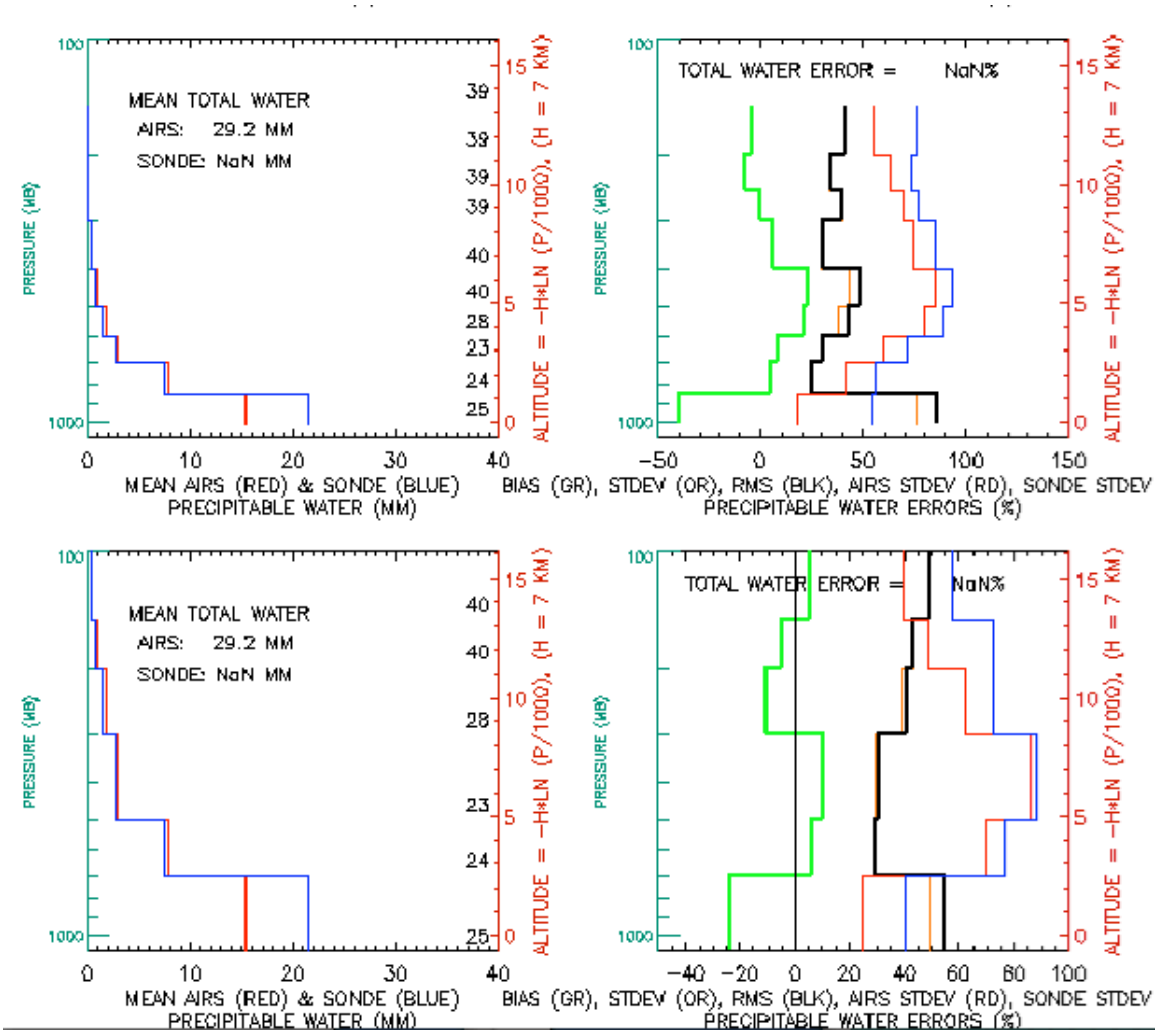

Figure 27. Water vapor profiles for CHE, at AIRS standard reporting levels (top) and in 2 km layers (bottom).

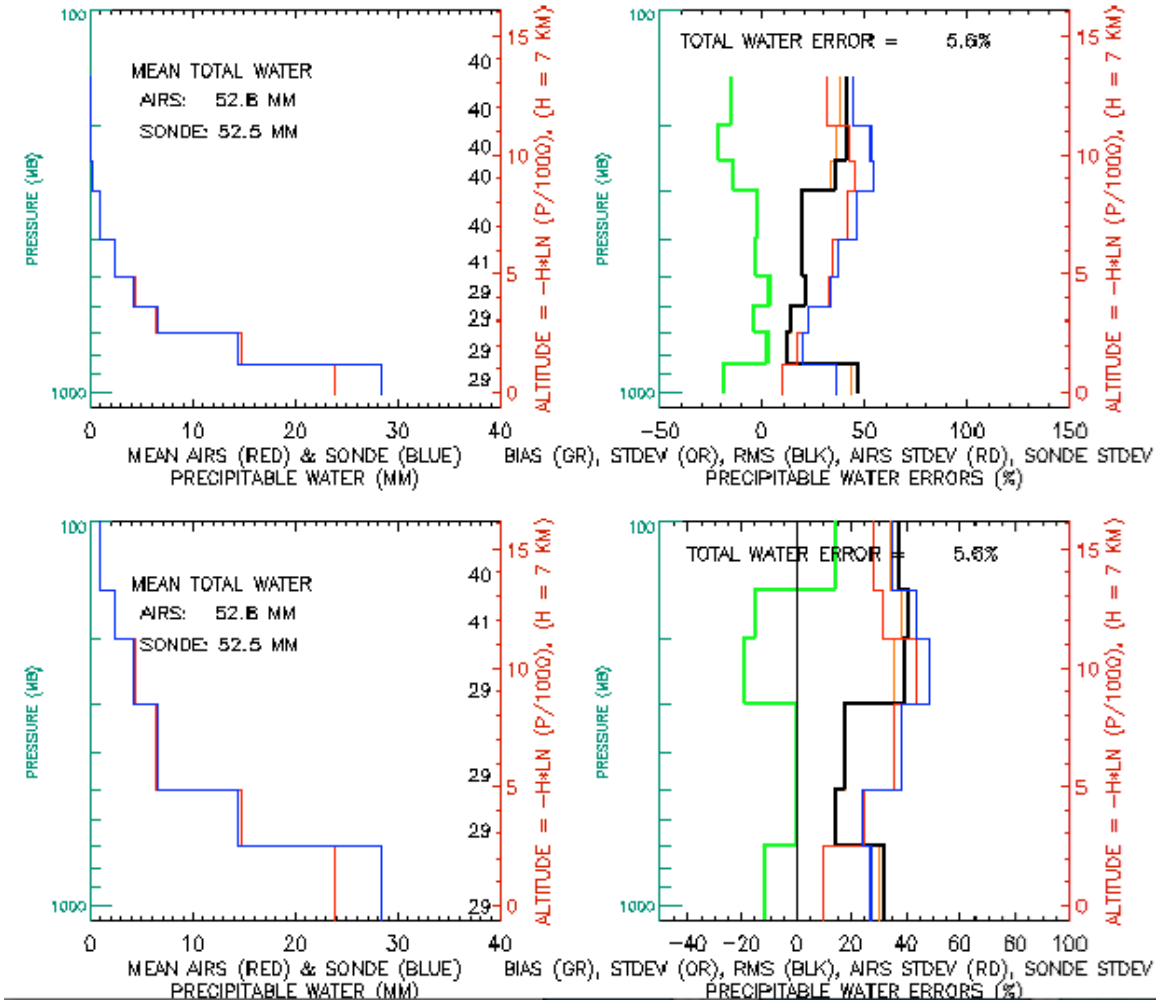

Figure 28. As Figure 27, for TWP

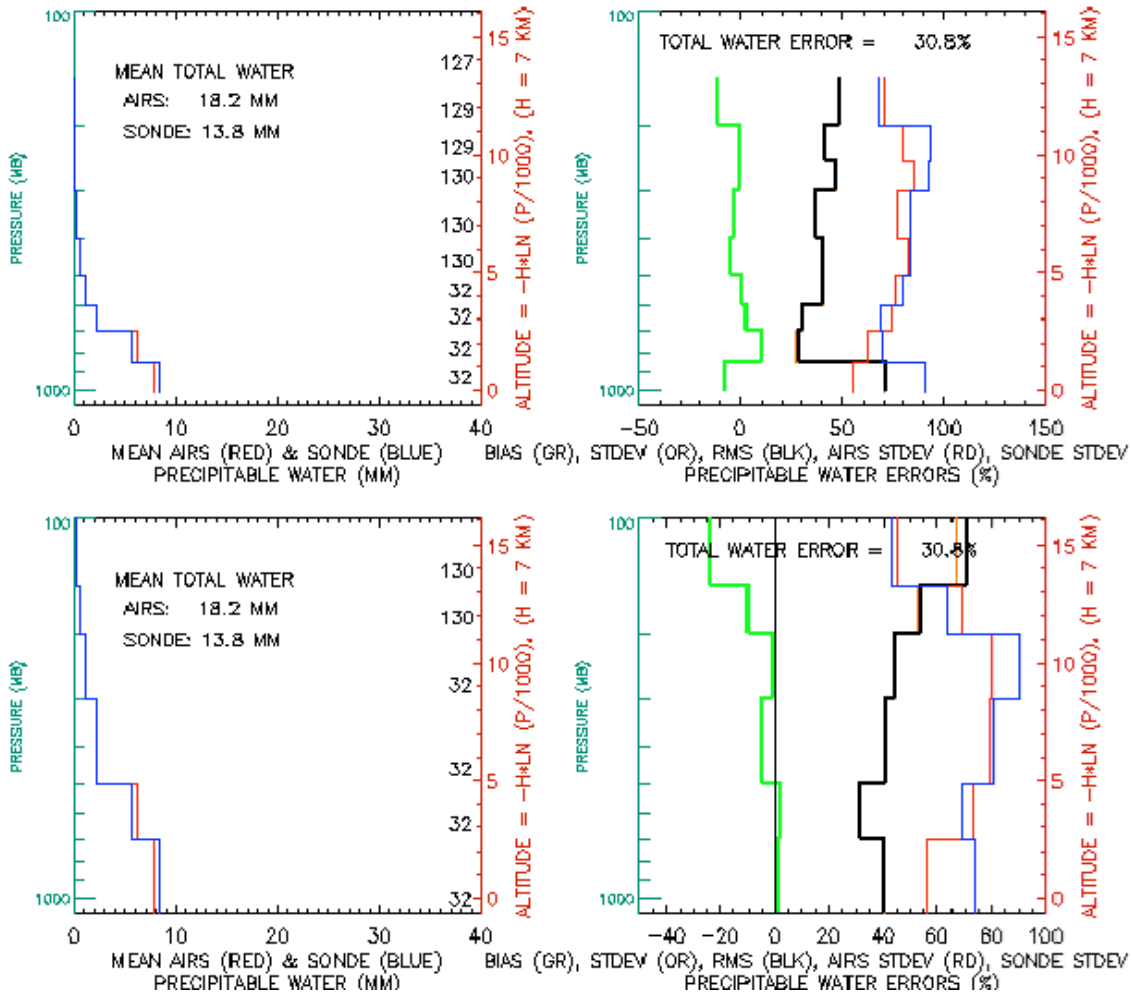

Figure 29. As Figure 27, for SGP

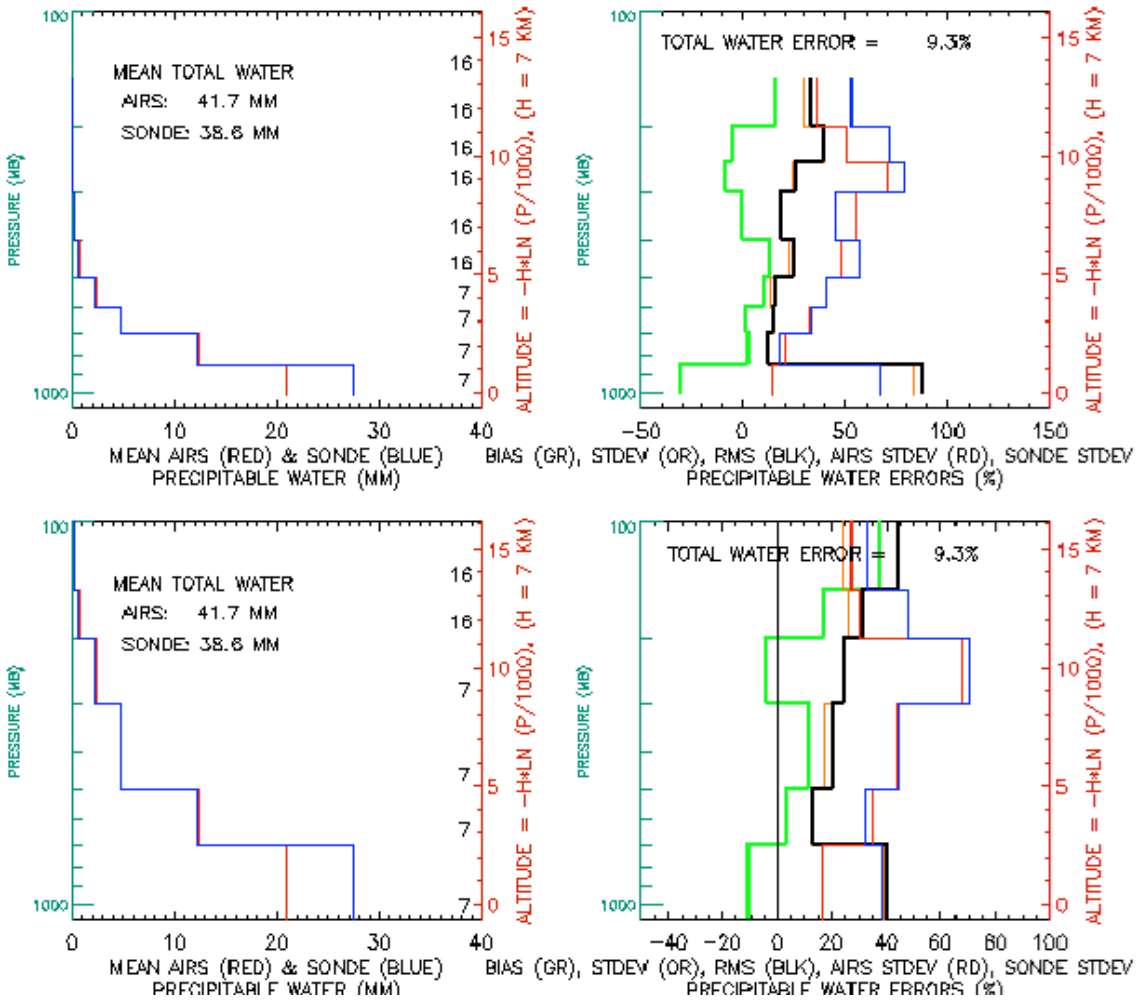

Figure 30. As Figure 27, for SCR

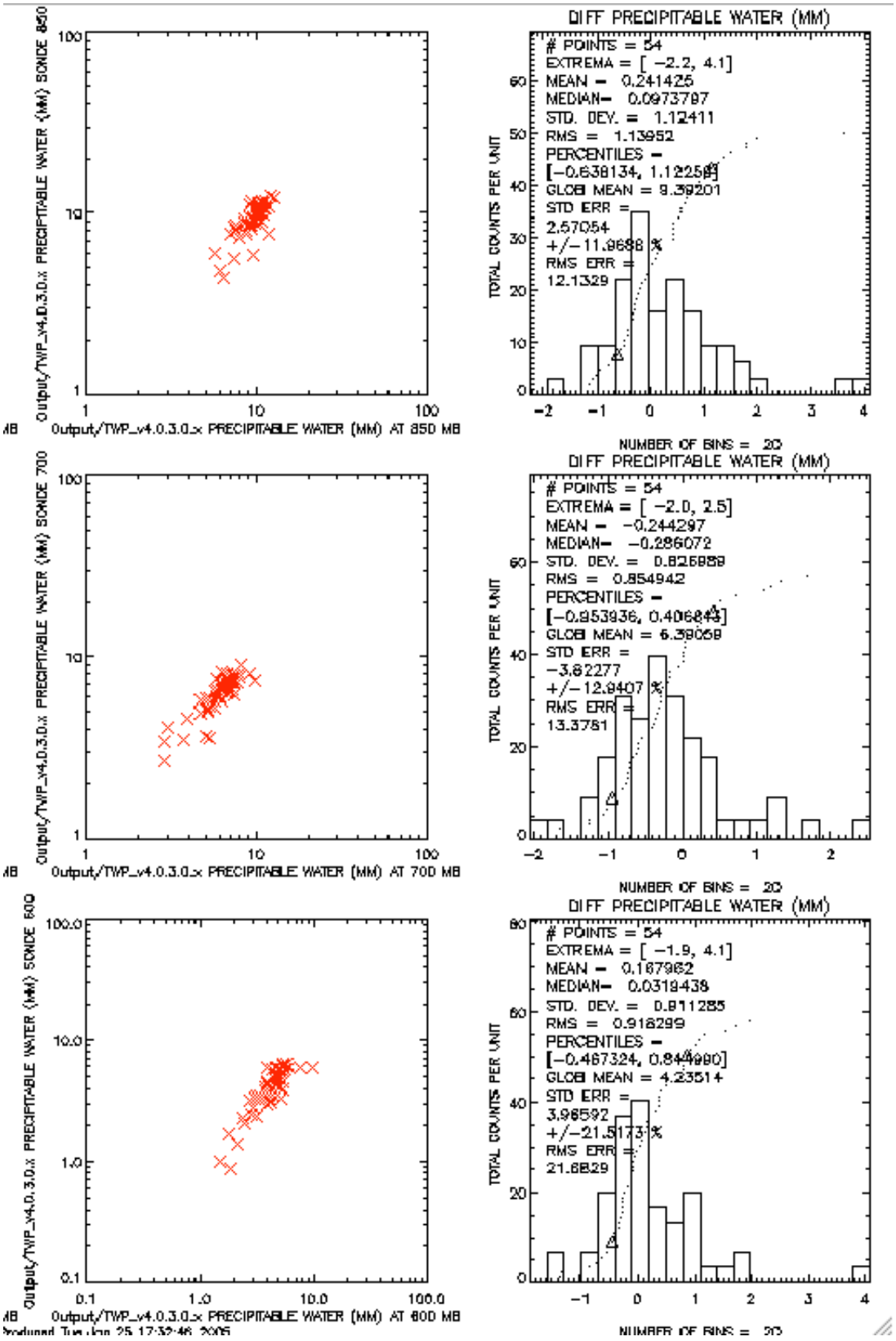

Figure 31. Scatterplots of precipitable water vapor for the TWP site for 850 to 600 mb.

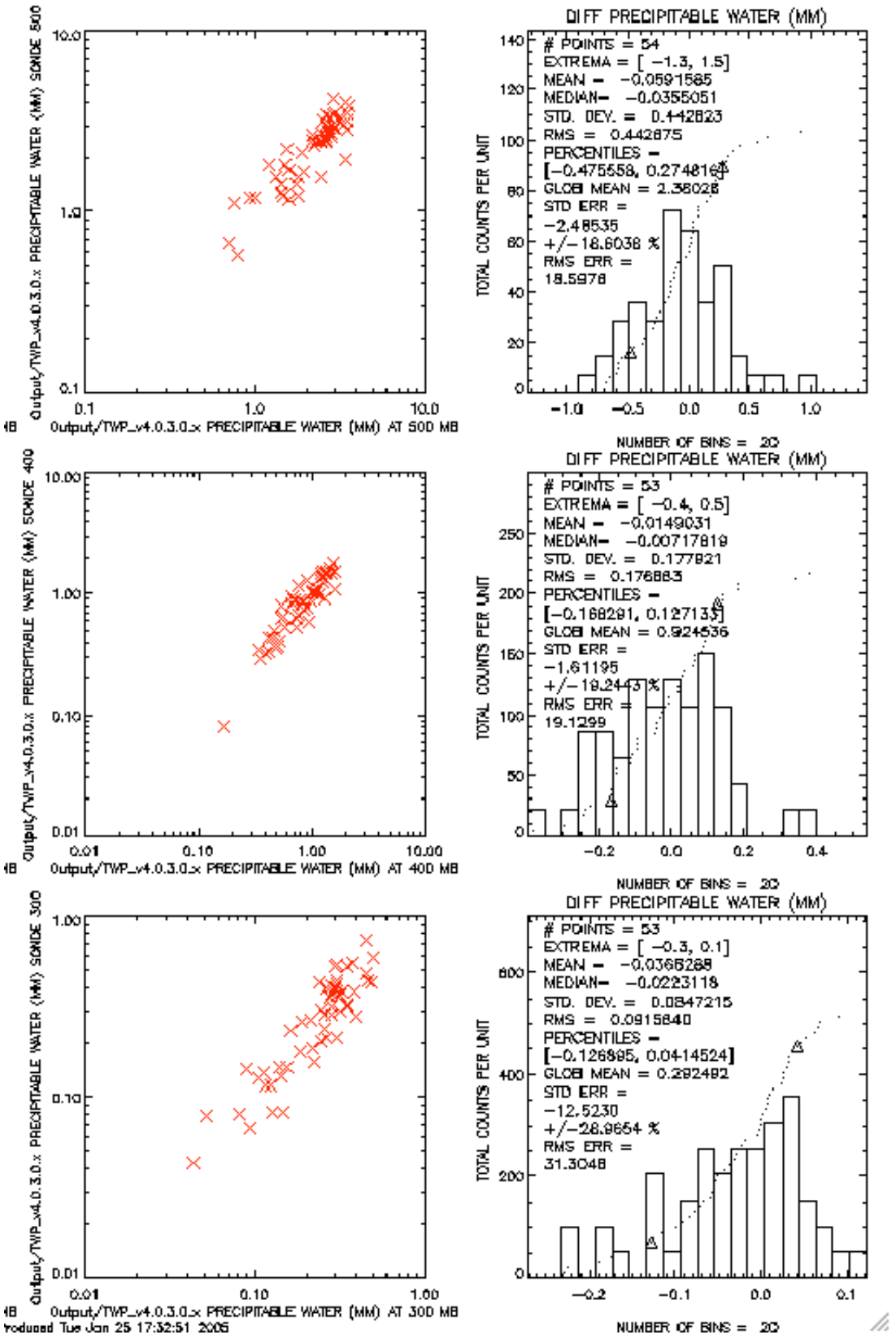

Figure 32. Scatterplots of precipitable water vapor for the TWP site for 500 to 300 mb.

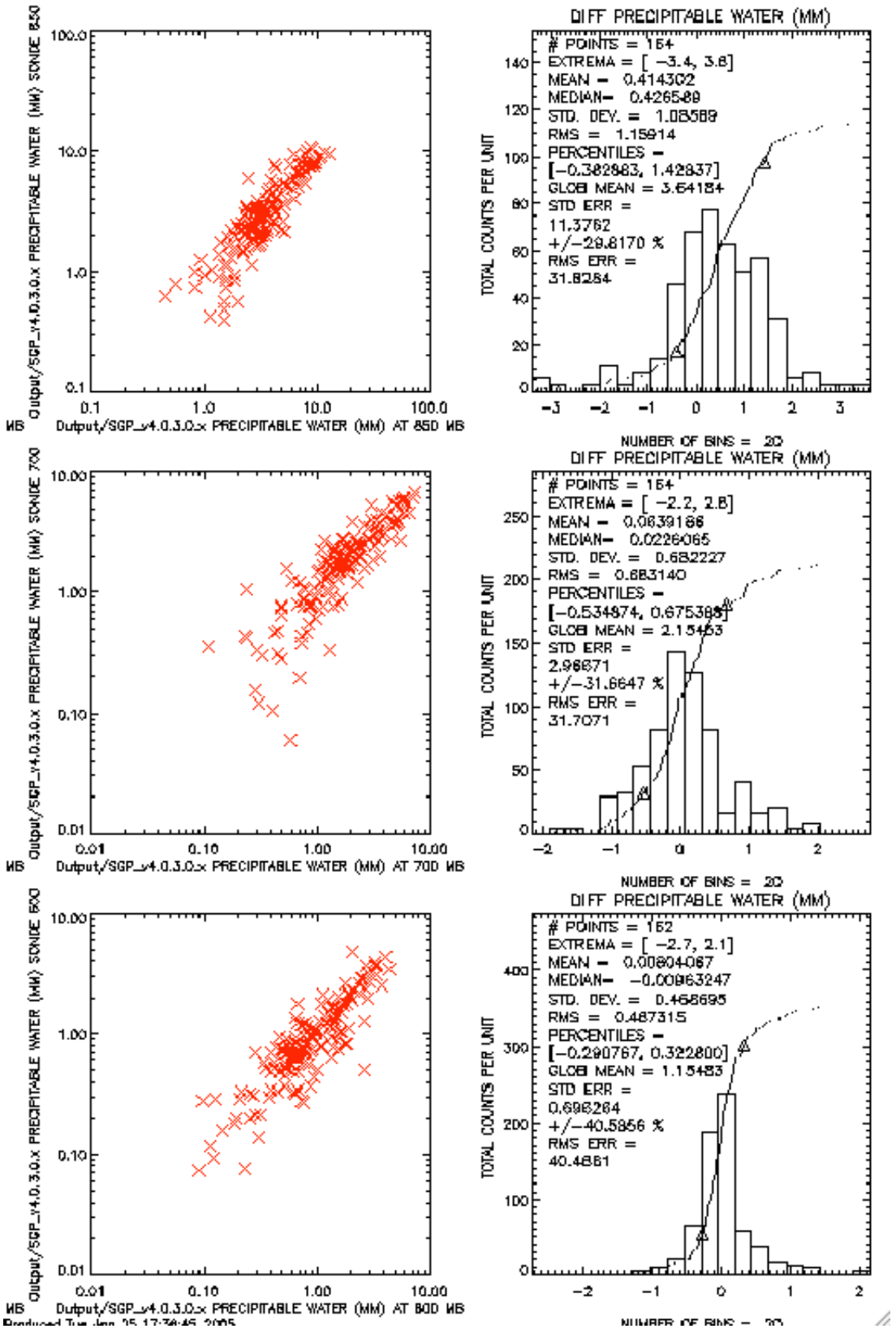

Figure 33. Scatterplots of precipitable water vapor for the SGP site for 850 to 600 mb.

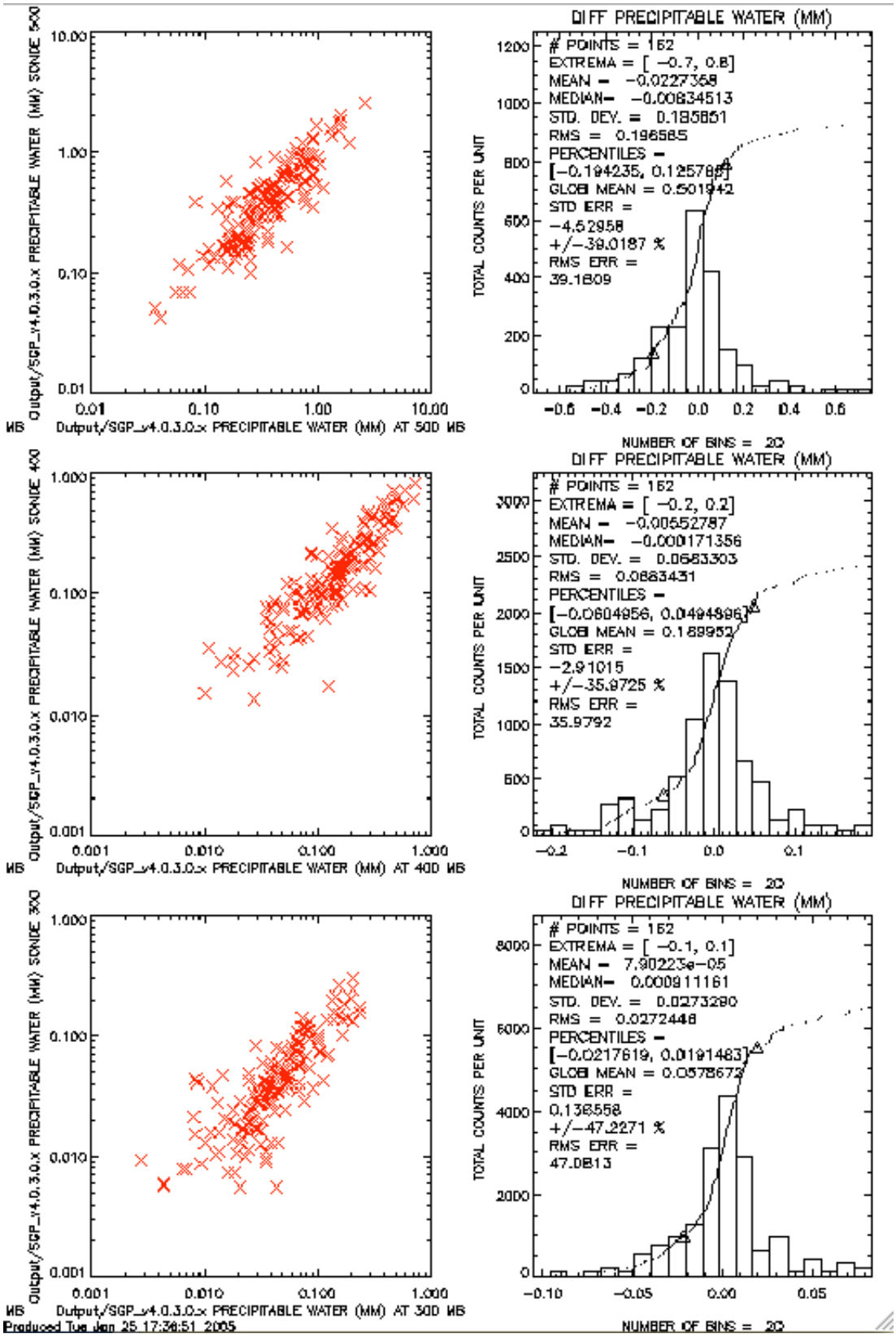

Figure 34. Scatterplots of precipitable water vapor for the SGP site for 500 to 300 mb.

3.6. Ozone Column and Profiles

Cloud-cleared spectra from AIRS are used to retrieve ozone profiles using the ν_3 band of ozone at a spectral resolution of ~ 0.85 cm^{-1} at ~1040 cm^{-1}. Figure 35 illustrates the channels used in the ν_3 band for both V3 and V4 of the AIRS retrieval. A significant motivation for the change in channels was to avoid weak, but highly temperature dependent CO_2 lines near the strong ozone lines near 1040 cm^{-1}. Figure 36 illustrates the daytime ozone total column retrieval between 50°S and 50°N for the Sept. 6, 2002 focus day.

As a check for ozone retrieval improvement between versions 3 and 4, we compare AIRS column ozone to gridded Version 8, Level 3 ozone columns retrieved by the Total Ozone Mapping Spectrometer (TOMS) on board the Earth Probe satellite [*McPeters et al.,* 1998]. AIRS V3.0.8 (similar to the version initially available at the Goddard DAAC) ozone is compared with Version 4 results. Daytime retrievals of column ozone from the September 6, 2002 focus day are compared if they fall within the TOMS grid of 1° in latitude by 1.25° in longitude, between 50°S and 50°N. Only data that "Qual_O3" flags equal to zero, indicating successful ozone retrieval, were used. Their relative difference is expressed as (AIRS - TOMS) / TOMS. For V3, the average difference for combined land and ocean retrievals is (8.3 ± 6.7)%, while for V4, the average difference is (1.6 ± 6.4)% (1σ). Table 10 shows the differences for land and ocean retrievals. In all cases, the biases have been significantly reduced.

Figure 37 illustrates the relationship between the AIRS-TOMS difference and the skin temperature for the Sept. 6, 2002 focus day. The color scale of the points is indicative of the land fraction, with red being over ocean and blue being over land. While V3 showed a significant correlation between these two variables, both the slope and the correlation coefficient have been reduced by more than an order of magnitude for V4. This is likely because of improvements in water vapor and temperature retrievals between the versions, as well as the channel re-selection.

Comparing additional V4 results to TOMS, again between 50°S and 50°N, average AIRS-TOMS differences for focus days from 2002 through 2004 are illustrated in Figure 38. AIRS total ozone columns tend to be within 2-3 % of TOMS over ocean and globally, and are biased high 0 – 5% compared to TOMS over land. Northern summer months tend to show higher biases than winter months (December, 2003 being a noticeable exception), with winter months showing slight negative biases over ocean.

Positive biases in the summer are also seen when comparing AIRS total column to Brewer spectrometer results from Arosa, Switzerland (Figure 39, left panel), and Dobson spectrometer results in Boulder, Colorado (Figure 39, middle panel). The seasonal variation appears to be somewhat less at Mauna Loa, Hawaii (Figure 39, right panel), although there is generally a positive bias. While AIRS is generally within 10% of the ground instruments about 60% of the time, the histogram of differences is not Gaussian, but tends to skew to positive biases. We note that comparison is complicated by the high altitude (~3.3 km for Mauna Loa, 1.5 km for Boulder, 0.7 m for Arosa) and mountainous topography of these sites. As the AIRS observation footprint is ~45 km, the

AIRS instrument *may* be sensitive to lower tropospheric ozone pollution sampled at regions and altitudes lower than that detectable at these sites.

Figure 40 illustrates AIRS profile retrievals compared to coincident ozonesondes. The center of the AIRS retrieval is within 100 km of the sonde launch site and 2 hrs within sonde launch. In the stratosphere, the (AIRS - Sonde) / Sonde difference is about –10%, while the differences in the free troposphere are on the order of 20 to 70%. As the comparison of the AIRS column with TOMS is reasonably good, the indication is that, to first order, the biases between the stratosphere and the troposphere cancel each other out in evaluating the total column.

Ongoing and future work:

- Further comparisons of AIRS tropospheric profiles with coincident ozonesondes, and stratospheric profiles from other instruments (e.g. OMI, SAGE, Umkehr, lidar).
- Full characterization of AIRS ozone vertical resolutions and errors.

AIRS - TOMS AIRS % ± 1σ	V3.0.8	V4.0.0
all regions	9.51 ± 6.68 (N = 56229)	1.65 ± 6.42 (N = 62381)
> 99% land	15.28 ± 7.69 (N = 8349)	3.83 ± 9.09 (N = 10096)
> 99% ocean	7.91 ± 5.40 (N = 41939)	0.99 ± 5.38 (N = 46051)

Table 10. Average (AIRS - TOMS) / TOMS difference (%) (1σ std. dev.) for Sept. 6, 2002 focus day.

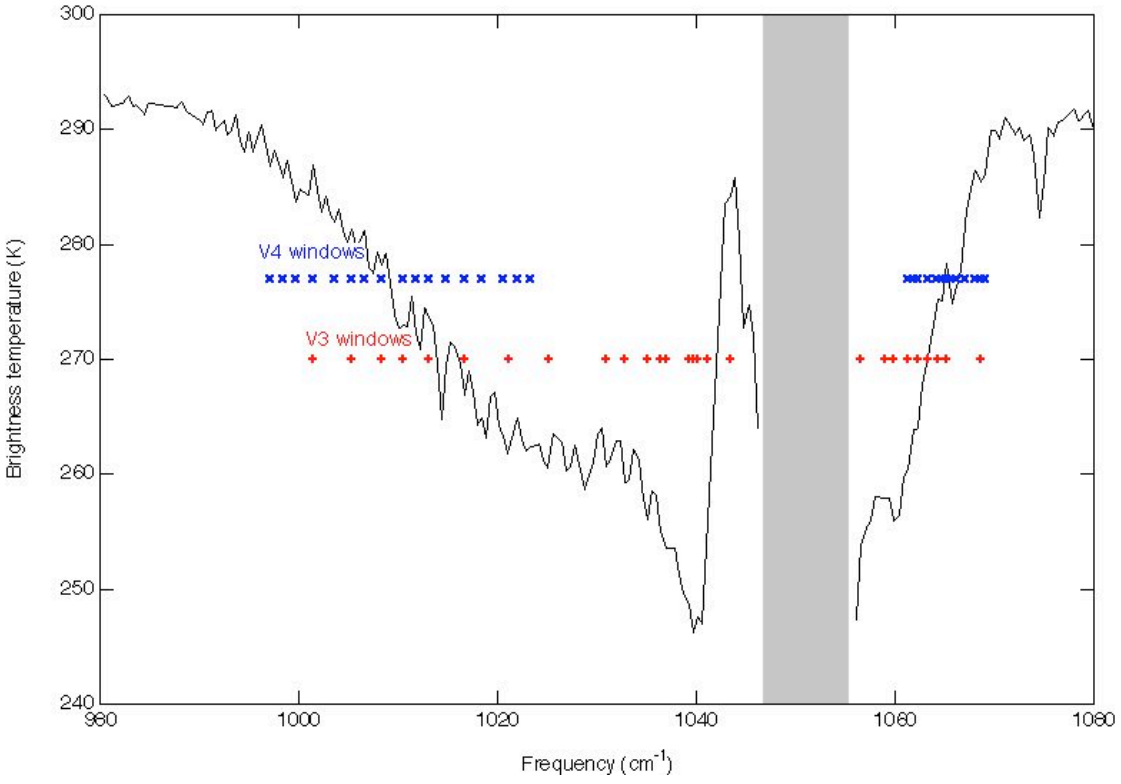

Figure 35. Sample AIRS partial spectrum. Channels used to retrieve ozone are indicated in blue (v4) and red (V3).

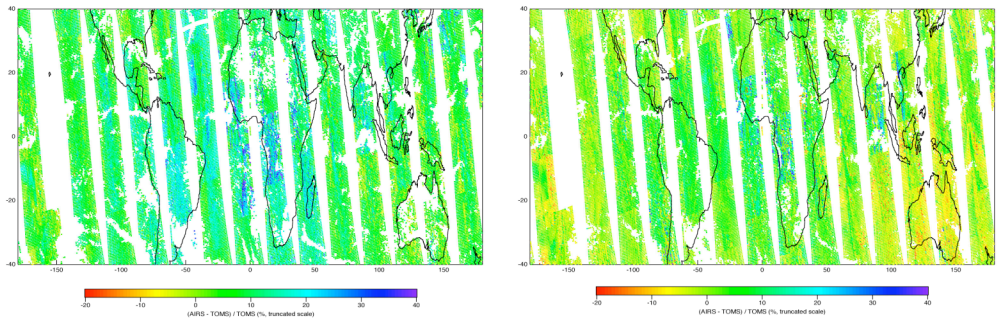

Figure 36. Average AIRS O3 column difference from TOMS for Sept. 6, 2002 using Version 3.0.8 (left panel), and for Version 4.0.0 (right panel).

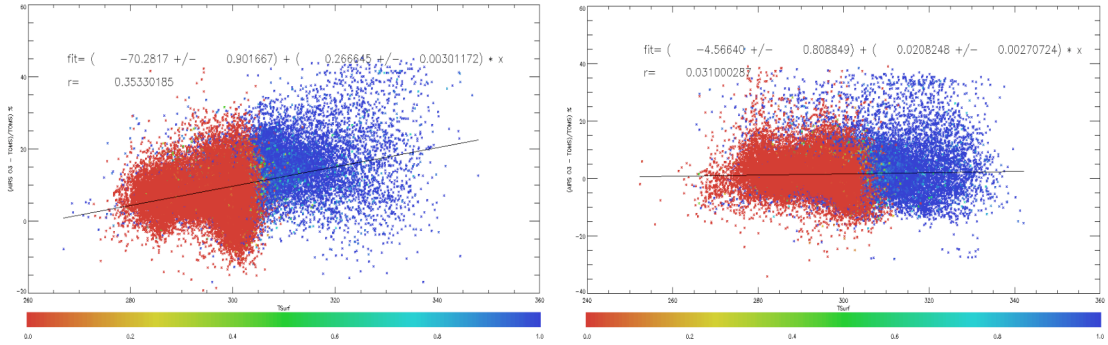

Figure 37. (AIRS - TOMS) / AIRS vs. retrieved skin temperature for Sept. 6, 2002 using Version 3.0.8 (left panel), and for Version 4.0.0 (right panel).

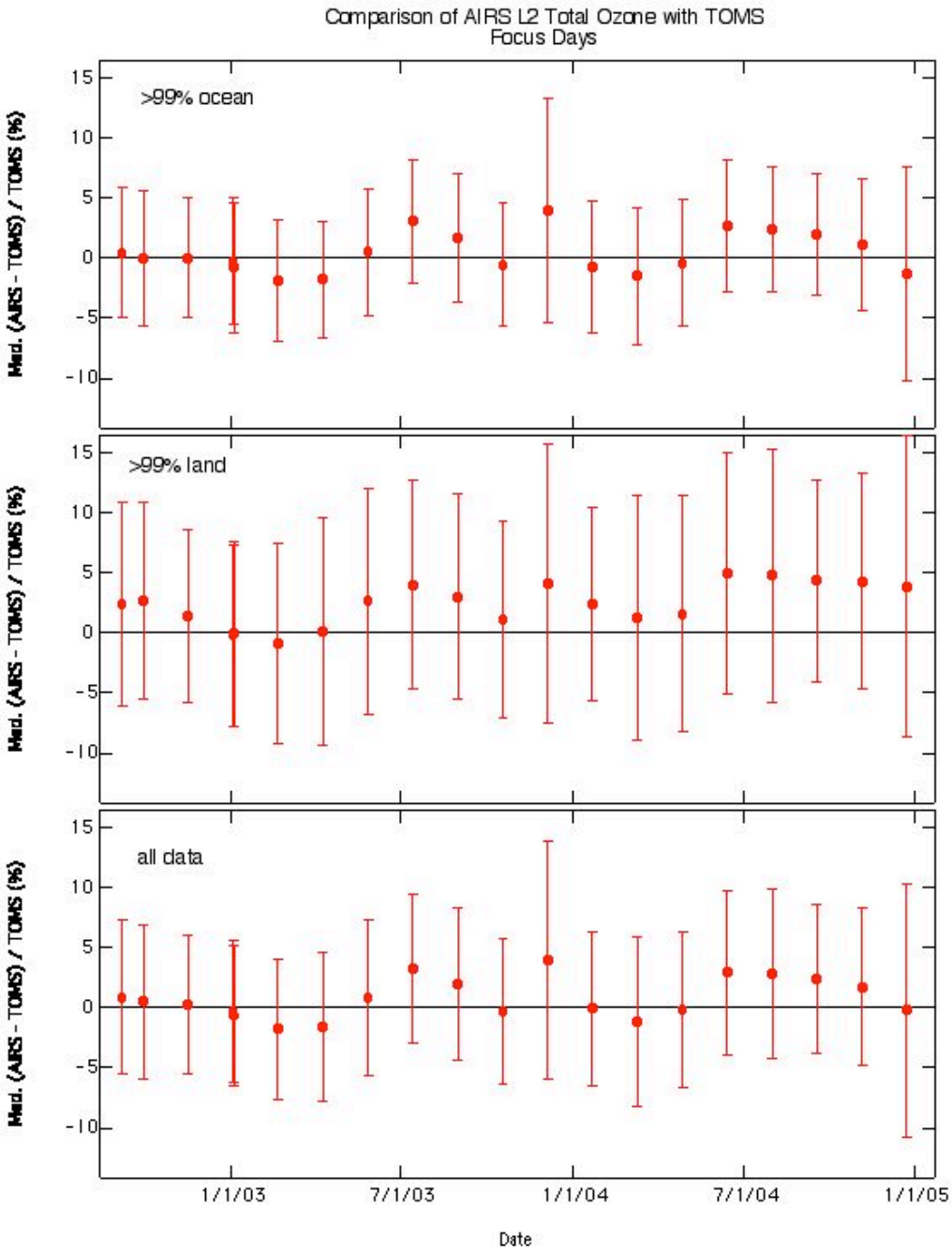

Figure 38. Relative differences of V4.0.0 AIRS to V8 TOMS, expressed as (AIRS-TOMS)/TOMS), for focus days between September 2002 and December, 2004. Data are daytime retrievals between 50°S and 50°N where "Qual_O3" = 0, indicating successful ozone retrieval. The upper panel is for ocean retrievals, the middle for land, and the bottom is for all cases

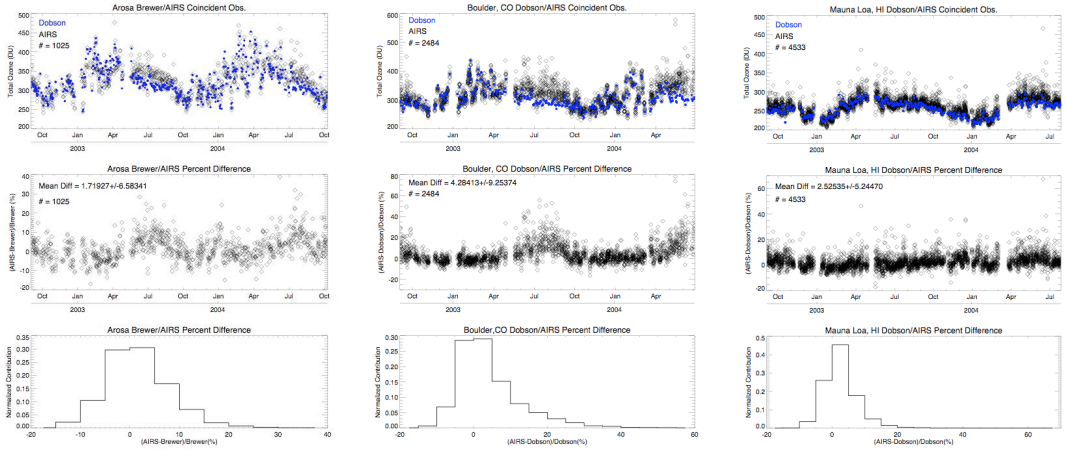

Figure 39. AIRS-Brewer comparisons over Arosa, Switzerland (left panel) and AIRS-Dobson comparisons over Boulder, CO and Mauna Loa, Hawaii (middle and right panels). The upper panels show total ozone retrievals, the middle panels show relative differences, and the bottom panels are histograms of the relative differences.

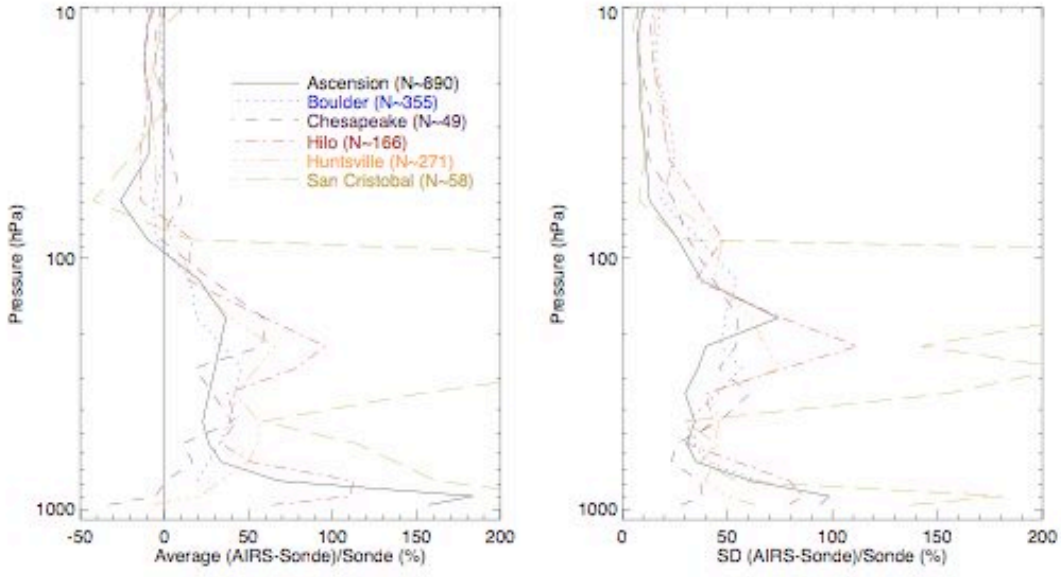

Figure 40. Average (AIRS - Sonde) / Sonde profiles for V4.0.0 (left panel) and standard deviations (right panel). "N" refers to the number of AIRS retrievals. Several AIRS observations may be matched up to a single ozonesonde. AIRS observations are made with 2 hours and 100 km of ozonesonde launch.

3.7. Cloud Fraction and Top Pressure

As part of the AIRS L2 standard product, cloud top pressure (CTP), cloud top temperature (CTT), and effective cloud fraction (CF) are reported at a maximum of two vertical levels (Susskind et al. 2003). Both CTP and CTT are representative of the AMSU footprint scale, with a nominal diameter of ~45 km near nadir view, while CF is representative of the AIRS footprint scale, with a nominal diameter of ~15 km near nadir view. As CTP is validated, the CTT is by default validated as well, as it is simply the temperature reported in the L2 TAirStd product interpolated to the pressure level of the cloud. For CF, comparisons to the Moderate Resolution Imaging Spectroradiometer (MODIS; Platnick et al. 2003) CF are in progress and the results will be presented elsewhere.

In this section we focus on the accuracy of the CTP estimates for both levels using the active sensor measurements at the Atmospheric Radiation Measurement (ARM) program Manus Island site in the Tropical Western Pacific, located at 2°S, 147.5°E. Since AIRS is sensitive to a broad spectrum of clouds, a comparison is made using the cloud boundaries value-added product (VAP; Clothiaux et al. 2000). The VAP combines the different capabilities of the micropulse lidar, millimeter-wave cloud radar, and laser ceilometer into a single cloud top and base product up to 10 cloud layers (Clothiaux et al. 2000), allowing for a comprehensive database for clouds with widely different vertical levels (ΔZ), optical depths (τ), and hydrometeor characteristics (phase, habit, size distribution).

Comparing a nearly instantaneous passive measurement from space at the scale of ~15 km or ~45 km with a surface-based, active point measurement is a very difficult task (Kahn et al., 2005). A useful, but not flawless, approach is to consider the surface measurements over a period of time for a given mean wind speed, in order to reproduce the spatial scale of the spaceborne measurement. For an idealized comparison of a homogeneous cloud scene, a minimum of the following must be true: (1) the wind speed and direction must be constant in space throughout the atmospheric column wherever the clouds reside, and must be constant with respect to time, (2) the cloud field must be static in time except for moving with the mean wind, and (3) the clouds properties (such as ΔZ, τ, particle size distribution, etc.) must be identical over the appropriate horizontal spatial scale and unchanging with time. In the real world, cloud properties are highly heterogeneous over ~45 km scales; clouds evolve (generate and dissipate, changing cloud properties) with time; many atmospheres are characterized by vertical wind speed and direction shear in the mean wind, which can change with time; perturbations from the mean wind speed and direction (e.g., via convection) makes a complicated wind flow pattern even more complicated. Additionally, the active surface-based and passive spaceborne measurements have different instrument sensitivities, and different algorithms are used to process the same type of cloud measurement, such as CTP. Under most circumstances, the surface-based measurement does not fall near the center of the AMSU footprint, further complicating the interpretation of the time–averaging of the VAP measurements. Geolocation errors with the spaceborne platform can lead to

discrepancies, especially near cloud edges and other areas with large horizontal gradients in changing cloud properties.

Keeping in mind the myriad of potential pitfalls when making comparisons of AIRS L2 CTP to the VAP at the ARM site, the results for 38 coincident measurements (8 ascending and 30 descending) are presented in Figure 41. This shows the agreement for three different time–averaging procedures for the VAP data: ± 24, 60, and 90 min either side of the coincident granule, for a total of 54, 126, and 186 min. The dashed line represents the conversion between pressure and altitude for a Standard Tropical atmosphere. The "error bar" in the horizontal direction is the 1–σ variation of the highest reported VAP cloud top height within its respective time window. The "error bar" in the AIRS CTP direction represents the relative uncertainty of the CTP. For the longer time average, the error bars are larger, consistent with more cloud top height variation over a larger spatial scale. In part d of Figure 41, a subset of the clouds presented in part c are shown for CF ≥ 0.15. The agreement overall is quite impressive for the optically thicker and more "prominent" clouds, with the error bars in the horizontal direction intersecting the line of agreement in most cases, and less so in the vertical direction. As a whole, the larger horizontal error bars are associated with poorer agreement, and vice-versa, well within expectations for heterogeneous cloud scenes.

Returning to Figure 41, there are several clouds with CF < 0.15 that are in poorer agreement with the VAP measurements (not all are in poor agreement). This may in part be due a lack of sensitivity of the lidar to the thinnest cirrus clouds at high altitude, and thresholds used in the VAP algorithm (K. N. Liou, personal communication). Indeed, manual inspection of coincident MODIS-Aqua Channel 31 radiances indicates the presence of some thin cirrus in several of the instances of disagreement between AIRS CTP and the VAP. Further investigation using the raw lidar profiles is in progress in order to determine if any of these cases may be spurious retrievals of cloud via the AIRS retrieval algorithm, or are mostly due to undetected thin cirrus in the VAP.

Comparisons of the lower layer AIRS CTP to the ARM VAP site has proven to be more difficult than the upper layer CTP. This may be true for many (speculative) reasons: (1) most of the time there isn't necessarily one or two very well-defined uniform cloud layers, (2) the lowest clouds have a BT similar to that of the surface, leading to a very low BT contrast and a large difficulty in cloud retrievals (Susskind et al. 2003), (3) the lowest cumulus clouds tend to be more broken and spotty than the higher clouds, and (4) the cumulus clouds may have some development related to Manus Island itself, leading to a discrepancy of the low cloud frequency in the VAP and over the AMSU footprint. Case-by-case comparisons show some promising low cloud CTP retrievals in the presence of higher cloud, and in other cases, are missed by AIRS, or are not seen in the VAP (not shown).

In order to present a general picture of the frequency of low clouds detected at Manus Island, histograms of cloud frequency are binned into 1 km increments (0–1, 1–2, … , 19–20 km) and are shown in Figure 42. The results are for the VAP over the 3 time–averaging procedures, and for the AIRS CTP for both layers in the cases shown in Figure 41. Despite the limited number of cases analyzed here, the general three-peak structure (1–2, 6 and 13–14 km) is consistent with previous results for nearby Nauru Island (Comstock and Jacob 2004). The three-peak structure in the AIRS histogram is not clearly seen, although the total number of cloud observations totals only several dozen,

and there are likely too few cases to represent a statistically meaningful distribution. However, there is a pronounced peak in cloud frequency near the surface, consistent with the ability of AIRS to sense an additional cloud layer below a semi-transparent higher cloud layer. The peak near 13–14 km in the VAP data is not seen in the AIRS data; this could be explained in part by numerous thin cirrus cases reported at higher levels than seen in the VAP, smoothing the peak of the histogram. For the cases with CF ≥ 0.15 the case-by-case comparisons are much better than the histograms imply. The peak in midlevel clouds near 6 km seen in the VAP is not immediately evident in the AIRS data. One possible explanation is due to the fundamental limitation of AIRS to two CTP layers, even though frequently 3 or more layers are observed simultaneously. In effect, the retrieval may miss many of these clouds.

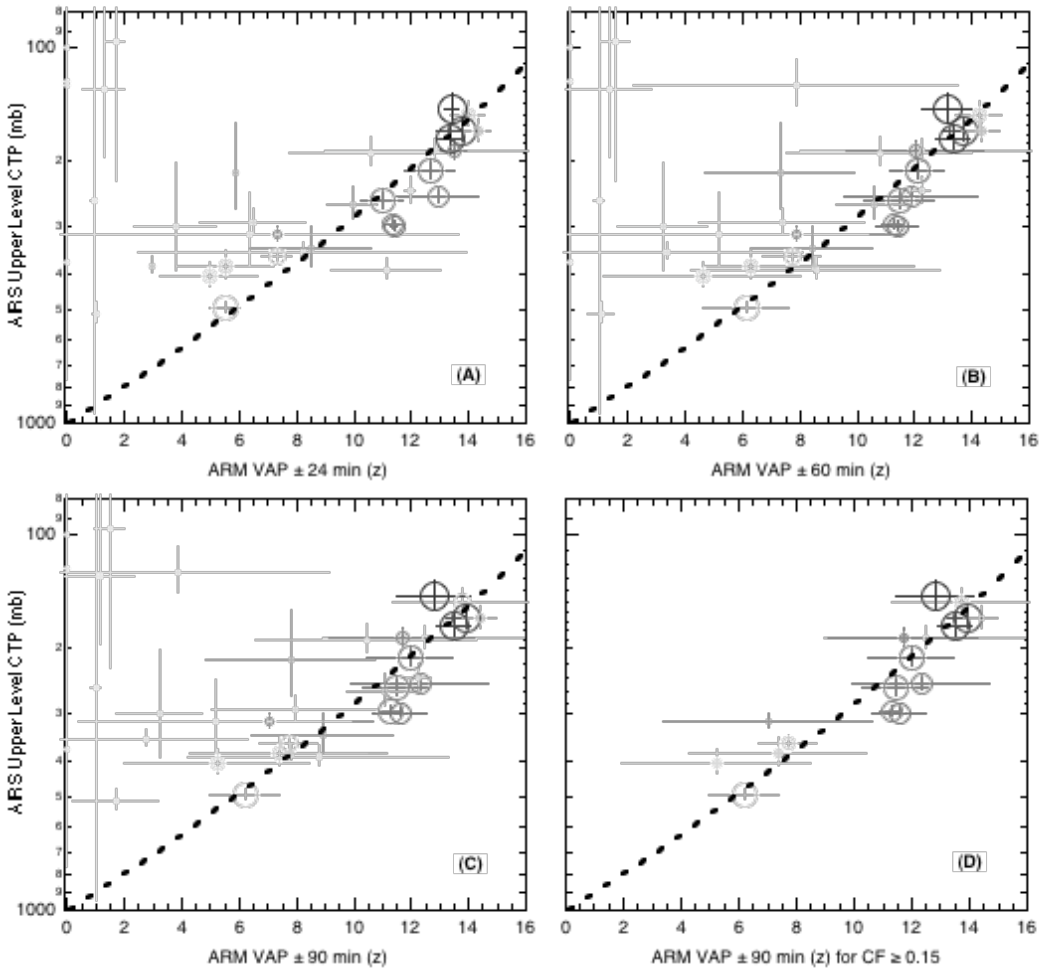

Figure 41. Scatter plot of AIRS L2 upper CTP (in millibars) versus the highest average cloud top in the cloud boundaries value-added product (VAP; Clothiaux et al. 2000) at the Atmospheric Radiation Measurement (ARM) program Manus Island, for a total of 39 day and night cases from May–September 2003. (A) ARM cloud top observations averaged 24 min before and after time of coincident granule, plus 6 min of granule time, for a total of 54 min. (B) Same as (A), except for 60 min, for a total of 126 min. (C) Same as (A), except for 90 min, for a total of 186 min. (D) Subset of (C) for CF ≥ 0.15 averaged over AMSU field of view. Bars in vertical direction are the reported AIRS upper level CTP uncertainties (in mb). Bars in horizontal direction are the 1–σ values on the highest reported cloud height in the VAP (not including clear sky observations). Diameter of circles proportional to AMSU field-of-view averaged CF, with largest (smallest) circles near 1.0 (0.0). Grayscale proportional to brightness temperature at 960 cm^{-1}, where black is ≈ 200 K and light gray is ≈ 300 K. The dashed line in the diagram represents the equivalent between height and pressure in a Standard Tropical Atmosphere with H ≈ 8 km.

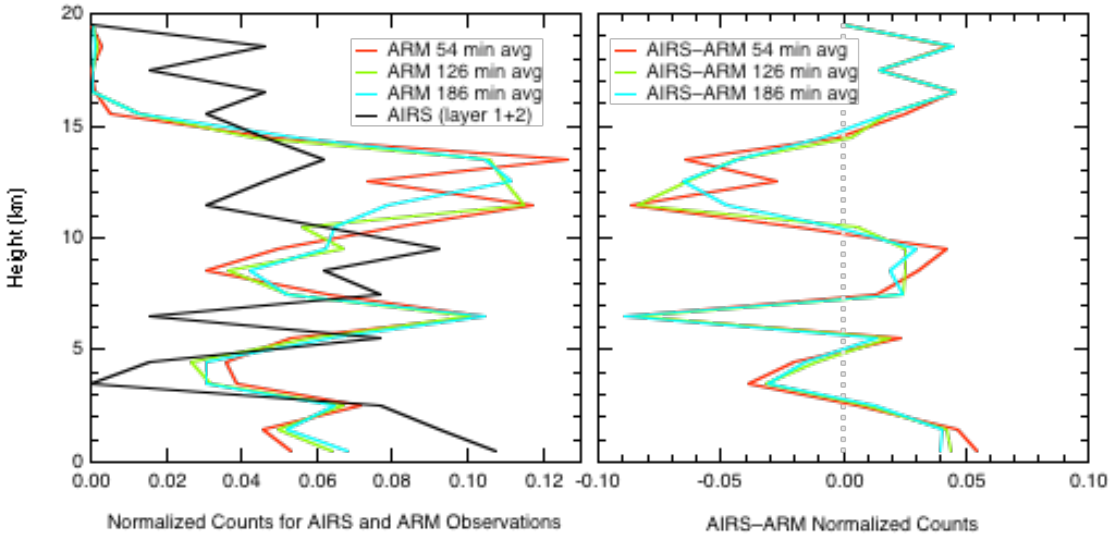

Figure 42. (a) Frequency histogram of cloud occurrence for the Manus Island VAP and AIRS CTP for both layers in vertical 1 km bins, normalized by the total number of cases. (b) Difference plot between the AIRS CTP and ARM VAP histograms.

List of Acronyms

ADFM	AIRS Design File Memorandum
AIRS	Atmospheric Infrared Sounder
AMSR-E	Advanced Microwave Scanning Radiometer
AMSU	Advanced Microwave Sounding Unit
ARM	Atmospheric Radiation Measuring
CF	Cloud Fraction
CHE	Chesapeake Light Platform
CTP	Cloud Top Pressure
ECMWF	European Center for Mediumrange Weather Forecasting
GTS	Global Telecommunications System
HIS	High-resolution Infrared Sounder
HSB	Humidity Sounder for Brazil
IEEE	Institute of Electrical and Electrons Engineers
M-AERI	Marine-Atmospheric Emitted Radiance Interferometer
NCEP	National Center for Environmental Prediction
NAST-I	NPOESS Aircraft Sounder Testbed - Infrared
NOAA	National Oceanic and Atmospheric Administration
RMS	root-mean-square
PGE	Product Generation Executable
RTG	Real Time Global
SCR	San Cristobal, Galapagos
SGP	Southern Great Plains
S-HIS	Scanning High-resolution Interferometer Sounder
SST	Sea Surface Temperature or Surface Skin Temperature
TOA	Top of Atmosphere
TOMS	Total Ozone Mapping Spectrometer
TWP	Tropical Western Pacific
UCSB	University of California at Santa Barbara

4. References

Aumann, H. H., M. T. Chahine and D. Barron, "Sea Surface Temperature Measurements with AIRS: RTG.SST comparison", SPIE 48th International Symposium on Optical Science and Technology, San Diego, CA, 3 August 2003.

Aumann, H. H., M. T. Chahine, C. Gautier, E. Kalnay, L. M. McMilllin, H. Revercomb, P. W. Rosenkranz, W. L. Smith, D. H. Staelin, L. L. Strow and J. Susskind, "AIRS/AMSU/HSB on the Aqua mission: design, science objectives, data products and processing", *IEEE Trans. Geosci. Remote Sensing*, vol. 41, pp. 253-264, Feb. 2003a.

Clothiaux, E.E., T.P. Ackerman, G.G. Mace, K.P. Moran, R.T. Marchand, M.A. Miller, and B.E. Martner (2000), Objective determination of cloud heights and radar reflectivities using a combination of active remote sensors at the ARM CART sites, *J. Appl. Meteor., 39*, 645–665.

Comstock, J.M., and C. Jacob (2004), Evaluation of tropical cirrus cloud properties derived from ECMWF model output and ground based measurements over Nauru Island, *Geophys. Res. Lett.*, *31*, L10106, doi:10.1029/2004GL019539.

Fetzer, E. J, H. H. Aumann, F. Chen, L. Chen, S. Gaiser, D. Hagan, T. Hearty, F. W. Irion, S.-Y. Lee, L. McMillin, E. Olsen, H. Revercomb, P. Rosenkranz, D. Staelin, L. Strow, J. Susskind, D. Tobin, and J. Zhou. Validation Of AIRS/AMSU/HSB Core Products for Data Release Version 3.0, August 13, 2003, JPL D-26538, 79 pages. Available online at http://daac.gsfc.nasa.gov/atmodyn/airs/.

Fetzer, E., L. McMillin, D. Tobin, M. Gunson, H. H. Aumann, W. W. McMillan, D. Hagan, M. Hofstadter, J. Yoe, D. Whiteman, R. Bennartz, J. Barnes, H. Vömel, V. Walden, M. Newchurch, P. Minnett, R. Atlas, F. Schmidlin, E. T. Olsen, M. D. Goldberg, Sisong Zhou, HanJung Ding and H. Revercomb, "AIRS/AMSU/HSB validation", *IEEE Trans. Geosci. Remote Sensing*, vol. 41, pp. 418-431, Feb. 2003.

Fetzer, E. J. and E. T. Olsen, L. L. Chen, D. Hagan, L. McMillin, 2003: Validation of AIRS / AMSU / HSB retrieved products. *Proc of SPIE,* **5151**, 210.

Fetzer, E., J. Teixeira, E. Olsen, E. Fishbein, 2004: Satellite remote sounding of atmospheric boundary layer temperature inversions over the subtropical eastern Pacific. Geophys. Res. Lett., vol. 31, L17102, doi:10.1029/2004GL020174.

Fishbein, E. F., C. B. Farmer, S. L. Granger, D. T. Gregorich, M. R. Gunson, S. E. Hannon, M. D. Hofstadter, S.-Y. Lee, S. Leroy, and L. L. Strow, "Formulation and validation of simulated data for the atmospheric infrared sounder (AIRS)", *IEEE Trans. Geosci. Remote Sensing*, vol. 41, pp. 314-329, Feb. 2003

Gaiser, S. L., H. H. Aumann, L. L. Strow, S. E. Hannon, and M. Weiler, "In-flight spectral calibration of the atmospheric infrared sounder (AIRS)", *IEEE Trans. Geosci. Remote Sensing*, vol. 41, pp. 287-297, Feb. 2003.

Gautier, C., Y. Shiren, L. L. and M. D. Hofstadter, "AIRS vis/near IR instrument", *IEEE Trans. Geosci. Remote Sensing*, vol. 41, pp. 330-342, Feb. 2003.

Gettelman, A., E. M. Weinstock, E. J. Fetzer, F. W. Irion, A. Eldering, E. C. Richard, K. H. Rosenlof, T. L. Thompson, J. V. Pittman, C. R. Webster and R. L. Herman, 2004, Validation of satellite data in the upper troposphere and lower stratosphere with in-

situ aircraft instruments. *Geophys. Res. Lett.*, v. 31, L22107, doi:10.1029/2004GL020730.

Hagan, D., AIRS Design File Memorandum #637 March 14, 2003.

Hagan, D. and P. Minnett, "AIRS radiance validation over ocean from sea surface temperature measurements", *IEEE Transactions on Geosciences and Remote Sensing*, pp 432-441, 41, 2003.

Hagan, D. E.; Webster, C. R.; Farmer, C. B.; May, R. D.; Herman, R. L.; Weinstock, E. M.; Christensen, L. E.; Lait, L. R.; Newman, P. A., 2004: Validating AIRS upper atmosphere water vapor retrievals using aircraft and balloon in situ measurements Geophys. Res. Lett., Vol. 31, No. 21, L21103.

Kahn, B. H., A. Eldering, S. A. Clough, E. J. Fetzer, E. Fishbein, M. R. Gunson, S.-Y. Lee, P. F. Lester and V. J. Realmuto, "Near micron-sized cirrus cloud particles in high-resolution infrared spectra: an orthographic case study", *Geophys. Res. Letters*, vol. 30, no. 8, p. 1441, 2003.

Lambrigtsen, B. H., and R. V. Calheiros, "The humidity sounder for Brazil--an international partnership", *IEEE Trans. Geosci. and Remote Sensing, 41*, 2, pp 352-361, 2003.

Masuda, K., T. Takashima and T. Takayama, "Emissivity of pure and sea waters for the model sea surface in the infrared window region," *Remote Sens. Environ.*, vol 24, pp 313-329, 1988.

McPeters, R. D. et al., "Earth Probe Total Ozone Mapping Spectrometer (TOMS) Data Products User Guide," NASA Technical Publication 1998-206895, NASA Goddard Space Flight Center, Greenbelt MD, 1998.

E. Olsen, H. Aumann, S. Broberg, L. Chen, D. Elliott, E. Fetzer, E. Fishbein, S. Friedman, S. Gaiser, S. Granger, M. Kapoor, B. Lambrigtsen, S.-Y. Lee, S. Licata and E. Manning. AIRS/AMSU/HSB Version 4.0 Data Release User Guide, February 28, 2005, 70 pages.

E. Olsen, E. Fetzer, S.-Y. Lee, and E. Manning. AIRS/AMSU/HSB Version 4.0 Level 2 QA Quick Start, February 28, 2005, 10 pages.

Pagano, T. S., H. H. Aumann, D. E. Hagan and K. Overoye, "In-flight spectral calibration of the atmospheric infrared sounder (AIRS)", *IEEE Trans. Geosci. Rem. Sens.*, 41, 265-273, 2003.

Platnick, S., M.D. King, S.A. Ackerman, W.P. Menzel, B.A. Baum, J.C. Riedl, and R.A. Frey (2003), The MODIS cloud products: Algorithms and examples from Terra, *IEEE Trans. Geosci. Remote Sensing*, *41*, 459–473.

Rosenkranz, P. W., Rapid radiative transfer model for AMSU/HSB channels, *IEEE Trans. Geosci. Rem. Sens.*, 41, 362-368, 2003.

Strow, L. L.., S. Hannon, S. DeSouza Machado, H. Motteler, and D. T. Gregorich, "An overview of the AIRS radiative transfer model", *IEEE Trans. Geosci. Remote Sensing*, vol. 41, pp. 274-286, Feb. 2003.

Strow, L. L.., S. Hannon, M. Weiler, K. Overoye S. L. Gaiser and H. H. Aumann, "Prelaunch spectral calibration of the Atmospheric Infrared Sounder", *IEEE Trans. Geosci. Remote Sensing*, vol. 41, pp. 303-313, Feb. 2003.

Susskind, J., C. Barnet and J. Blaisdell, "Retrieval of atmospheric and surface parameters from AIRS/AMSU/HSB in the presence of clouds", *IEEE Trans. Geosci. Remote Sensing*, vol. 41, pp. 390-409, Feb. 2003.